

Harvesting Vibrational Energy



WPI

Harvesting Vibrational Energy

A Major Qualifying Project Report
Submitted to the Faculty of the
WORCESTER POLYTECHNIC INSTITUTE
in partial fulfillment of the requirements for the
Degree of Bachelor of Science in Mechanical Engineering

By: Laura Carlson
Theresa Cloutier
Allanah Kalka-Riffel
Kishan Patel
Kevin Pawlak

Date: 03/15/2019

Report Submitted to:

Professor Brian Savilonis
Mechanical Engineering Department
Worcester Polytechnic Institute

Abstract

With the increasing push for sustainability, more industries are looking for ways to incorporate renewable energy. With the amount of machinery being used around the world, researchers are beginning to investigate machine vibrations as a renewable energy source. This project aimed to create a working prototype that demonstrates the ability of piezoelectric materials to generate electricity from these vibrations. The final prototype design not only harvested electricity, but also successfully dampened excess vibrations to protect the machinery. The design included a square tile that housed the piezoelectric circuit, dampening subsystem, and supported the blender. Upon final testing, the prototype was able to charge a capacitor. With a dampening system, the prototype generated 8 millivolts.

Acknowledgements

This project was produced with the aid of many different people. Our team would like to take this space to thank them.

First and foremost, our team would like to thank Professor Savilonis, our faculty advisor. He was supportive and gave us direction throughout the entire process. He pushed us to think outside of our comfort zone and guided us from the design process until the final submission. We greatly appreciate everything he did for us and all of the resources he provided.

We would also like to thank Professor Furlong for his invaluable information on accelerometers and LabVIEW. He gave initial direction into creating our LabVIEW program and even provided a few 2-axis accelerometers for our initial testing. From his experience in the field, we designed and created a successful prototype.

Prof. Scarpino was also instrumental in the troubleshooting our LabVIEW program and we would like to thank him for all of the advice that he provided.

Our team also thanks Mr. Cloutier for his aid in obtaining, implementing, and analyzing and the data collected with the 3-axis accelerometer evaluation board.

Our thanks go to Ms. Furhman as well for all of the support she provided during the ordering and obtaining of the parts and components required during the production of this project.

Lastly, we would like to thank Peter Hefti for his consistent help with the lab equipment.

Table of Contents

Abstract	2
Acknowledgements	3
Table of Contents	4
List of Figures	6
List of Tables	7
Introduction	8
Background	9
Vibrations	9
Energy Harvesting Methods	10
Electrostatic	10
Triboelectric	11
Electromagnetic	12
Piezoelectric	14
Piezoelectric Circuitry	16
Methods of Vibration Transference in a Piezoelectric Setup	17
Past Research Applications using Piezoelectric Systems	18
Issues with current harvesting methods and applications	19
Methodology	20
Design Specifications	20
Preliminary Analysis	20
Tachometer Testing	20
Preliminary Accelerometer Testing	21
Final Accelerometer Testing	22
Design	28
Prototype One	28
Prototype Two	30
Prototype Three	32
Results	34

Spring Incorporated Version	34
Spring-less Version	35
Power Output.....	36
Conclusion	39
Manufacturing Considerations.....	41
Assembly Procedure.....	42
Automating and Improving the As-Is Process	43
Energy Analysis and Application.....	44
Expanded Manufacturing Applications.....	45
Impact	47
References.....	48
Appendices.....	54
Appendix A: Blender Motor Speed Test Procedure.....	54
Appendix B: Accelerometer Test Procedure.....	56
Preliminary Setup.....	56
Experimental Testing with Cornstarch.....	59
Experimental Testing with Water	60
Experimental Testing with Accelerometer on Prototype	61
Appendix C: Piezoelectric Test Procedure for Voltage Testing	63
Preliminary Setup.....	63
Experimental Testing	63
Appendix D: Specifications Sheets.....	65

List of Figures

Figure 1: The Triboelectric Process [40]	12
Figure 2: Electromagnetic Generator Schematic [41]	13
Figure 3: Direct and Converse Piezoelectric Effect [65]	14
Figure 4: Signal Response from a Diode [38]	16
Figure 5: Full Wave Bridge Rectifier Circuit [39].....	17
Figure 6: Initial Experiment Wiring Setup	21
Figure 7: Pin Schematic of Evaluation Board with ADXL326 Accelerometer [66]	22
Figure 8: Wiring Configuration of EVAL-ADXL326Z to DAQ Unit with AA Battery Input Voltage.....	23
Figure 9: Screenshot of LabVIEW Program (Cornstarch, Liquify Speed, Z-Axis, Trial 1).....	23
Figure 10: Accelerometer Axis Orientation.....	24
Figure 11: Position 1	24
Figure 12: Position 2.....	24
Figure 13: Sample Displacement Curve (Cornstarch, Liquify Speed, Z-Axis, Trial 1)	27
Figure 14: Sample Frequency FFT Graph (Cornstarch, Liquify Speed, Z-Axis, Trial 1)	28
Figure 15: Base box with Ball Bearing Transfer Units.....	29
Figure 16: Prototype One.....	29
Figure 17: Energy Harvesting Circuit.....	31
Figure 18: Isometric View of CAD drawing of Prototype Two	31
Figure 19: Side View of the CAD drawing of Prototype Two	31
Figure 20: Photo of Prototype Two	32
Figure 21: Prototype Two Circuit Diagram	32
Figure 22: Prototype Three with the circuit outside for testing purposes.....	33
Figure 23: Close-up of piezoelectric stack, spring, and plate assembly (Damping Subsystem) ..	33
Figure 24: Spring Prototype Water Acceleration Graph.....	34
Figure 25: Spring Prototype Water Voltage Graph	34
Figure 26: Spring Prototype Cornstarch Acceleration Graph.....	35
Figure 27: Spring Prototype Cornstarch Voltage Graph.....	35
Figure 28: Spring-less Prototype Water Acceleration Graph	35
Figure 29: Spring-less Prototype Water Voltage Graph	35
Figure 30: Spring-less Prototype Cornstarch Acceleration Graph	36
Figure 31: Spring-less Prototype Cornstarch Voltage Graph	36
Figure 32: Proposed Circuit for Multiple Tile Platform	46

List of Tables

Table 1: Tachometer Results for each Speed.....	20
Table 2: Sample RMS Average of Acceleration (g).....	25
Table 3: Deflection Values	26
Table 4: Piezoelectric Materials Deflection Ranges.....	26
Table 5: Spring-less Power Output.....	37
Table 6: Springs Incorporated Power Output	38
Table 7: Testing Overview.....	39
Table 8: Bill of Materials.....	41

Introduction

Carbon dioxide levels have increased 100 parts per million in the past sixty years and the surface temperature of the world has increased by 1.62 degrees Fahrenheit [1]. If carbon dioxide levels continue to rise, the combination of burning fossil fuels and the greenhouse effect will increase sea levels [2]. Although these alarming statistics convey the negative impact of using fossil fuels as primary energy sources, they are also driving people to put more and more effort into optimizing other sources of renewable energy.

There are many fields of renewable energy such as wind, water, and solar, but there are also opportunities to harvest mechanical energy. Wind, water and solar power have been applied to large scale applications, but are limited since they are dependent on nature. If there is no wind or no sun, these sources cannot harvest energy [3]. Mechanical energy can be in many forms, including kinetic motion or vibrations. Many machines like cars, household appliances, and CNC machines in manufacturing plants vibrate from their various operations. These vibrations can be harnessed using different methods of energy harvesting. One example is a device that uses piezoelectric and solar cells to power an RF beacon. The power output recorded was $375 \mu\text{W}$ from an acceleration of 2.25 m/s^2 at 60 Hz, which corresponds to a displacement of $16 \mu\text{W}$ [51].

In order to harvest this vibrational energy, there has to be a generator that can convert the vibration frequency into electricity. There are three main types of generators: piezoelectric, electromagnetic, and electrostatic. A fourth type of generation, triboelectricity, is a recent addition and most of its work remains in the theoretical phase. All four methods use different mechanisms to create energy; piezoelectric generators are specific materials of a crystalline structure that generate an electric potential when subjected to a mechanical strain.

Electromagnetic generators use the interaction of a moving coil, caused by an external force, and a stationary magnet to create an electromagnetic field in which changes in the generated magnetic field induces an electric current [4]. Electrostatic energy harvesters use a variable capacitor between dielectric materials to convert the electrostatic mechanical energy into electrical energy [9]. The triboelectric effect is created when two dielectric materials, of opposing polarity, create an electrostatic charge by repeated contact and separation allowing for electrons to pass back and forth via electrodes [5].

The aim of this Major Qualifying Project was to create a prototype that can efficiently harvest the vibrational energy of a regular household blender using a piezoelectric system to illustrate the usefulness of vibrations and how they can be applied to larger systems such as CNC machining floors. All machinery exhibit vibrational energy. This allows for extensive research and design opportunities to create a design that has mechanical advantage to increase efficiency.

Background

Vibrations

Vibrations are classified as a form of mechanical energy and can be used to define the frequency of an object's oscillation. Vibrations occur with all bodies that have both mass and elasticity. Classifications used to generalize vibrations include forced and free. Free vibrations describe the system acting in response to itself, meaning that there are no external forces. In this type of system, vibrations will follow the systems natural frequency. Forced vibrations refer to when the system reacts to the exposure of an external force. When this occurs, the system will vibrate at the external forces frequency. If the external force frequency happens to coincide with the natural frequencies a phenomenon of resonance occurs. Resonance can prove to be dangerous, especially with structural elements like bridges or machinery because large oscillations may occur that can cause a system failure [37].

When there are repetitive oscillations in equal intervals of time, the system is termed to have periodic motion. Frequency (f) is the number of times an object moves through one full cycle over the course of one second. Frequency in this type of system can be determined using Equation 1, which is based on wave periods (T) [6].

$$f = \frac{1}{T} \quad (\text{eq.1})$$

Harmonic motion is the most basic form of periodic motion and can involve suspending a mass from a spring. In an ideal situation, springs are massless and frictionless, which means they would oscillate at the same frequency for an infinite amount of time. Equation 2 describes harmonic motion that oscillates continuously. The distance (x) the mass travels from its original location is referred to as the amplitude of oscillation and is represented by variable A in the equation. T refers to the period and this motion gets repeated when time (t) equals the period [37].

$$x = A \sin 2\pi \frac{t}{T} \quad (\text{eq.2})$$

Outside of an ideal situation, vibrations of an object will be affected by factors such as friction, air resistance and other outside sources. These factors contribute to the energy lost from the system and is referred to as damping. The damping force is an important parameter to understand for multiple calculations, including the resonant frequency, which is the natural frequency based on the physical qualities of the object that is vibrating [7] [8]. Natural frequency is the rate at which an object vibrates when it experiences an external force. However, once an object experiences a disturbance it will initially vibrate at its natural frequency until damping effects

begin to lower the amplitude. Equation 3 describes the undamped natural frequency of the system. Omega (ω) represents the natural frequency, while k and m represent the spring constant and mass, respectively.

$$\omega = \sqrt{\frac{k}{m}} \quad (\text{eq.3})$$

The damping force can be modeled for an object at any time to be directly proportional to its speed. Equation 4 depicts the differential equation that would be used along with the solution.

$$m \frac{d^2x}{dt^2} = -kx - b \frac{dx}{dt} \quad (\text{eq.4})$$

$$x = Ae^{\left(\frac{-b}{2m}t\right)} \cos(\omega't + \phi) \quad (\text{eq.5})$$

$$\omega' = \sqrt{\frac{k}{m} - \left(\frac{b}{2m}\right)^2} \quad (\text{eq.6})$$

$$\zeta = \frac{b}{2\sqrt{mk}} \quad (\text{eq.7})$$

In the equations 5-7 above, b represents the damping force proportionality constant, x represents the displacement of the object, and ϕ represents the phase angle. The damping coefficient, ζ , can be used to determine what kind of damping exists. Critical damping occurs when the coefficient equals one. This condition indicates that the object will change from oscillating to equilibrium quickly. Underdamping occurs when the coefficient is less than one; the object will oscillate with an amplitude that continues to decrease. Overdamping occurs when the coefficient is greater than one; the resistive forces are strong allowing the object to reach equilibrium much slower. Undamped occurs when the coefficient is equivalent to zero, an indication there are no resistive forces [52].

Energy Harvesting Methods

There are three common techniques that are used to convert mechanical energy into electricity: electromagnetic, piezoelectric, and electrostatic [9]. In addition, there is a newer technique, triboelectric, that has been used in proof of concepts.

Electrostatic

In order to convert mechanical energy into electrical energy, a variable capacitor is used. A capacitor consists of dielectric material between two metallic plates. A dielectric material acts as an insulator while the metallic plates act as conductors. Wires are attached to the conductors (called terminals) in order for the charge to flow into the electric circuit. An electric field is

created when a voltage is applied across the two conductive plates. On one side of the plate, positive charge will accumulate; the other plate will accumulate a negative charge. The accumulation of negative charge on one plate is considered charging and the release of this energy is considered discharging [10].

Capacitance is the amount of energy a capacitor is able to store and it is measured in farads, F . The larger the plates, the more energy can be stored. Capacitance can be increased by moving the plates closer together as the charges will have a stronger effect at a closer distance [11].

In the electrostatic model, the variable capacitor acts as an electromechanical transducer. A voltage is required across the capacitor for there to be electrical energy. Typically, a spring is used as a mechanical intermediate, which results in a resonating structure [9].

There are many different geometries that can be used to create an electrostatic system. The simplest to understand is a system of two parallel plate capacitors where one of the plates is fixed. The plate that is not fixed is free to move with the external resonant frequency. As this plate moves, the distance between the two plates varies, which in turn varies capacitance. Two other ways to achieve a similar effect is by variable area and variable dielectric constant [12]. Equation 8 depicts how energy (E) can be collected per cycle of movement when one of the plates is fixed. Q represents the charge. C_{min} represents the minimum capacitance and C_{max} represents the maximum capacitance.

$$E = \frac{1}{2}Q^2(1C_{min} - 1C_{max}) \quad (\text{eq.8})$$

In order to create energy from the charged capacitance, a conversion system is used. There are two commonly used conversion mechanisms, voltage-constrained and charge-constrained [12]. An electrostatic converter uses a mechanical medium and electric circuit to convert the external energy into electrical energy.

Triboelectric

Electric current is the flow of electrons through an electric circuit [13]. The movement of electrons is caused by the creation of a charge imbalance, or voltage [14]. In triboelectric nano-generators, this charge imbalance is created when two materials on opposite ends of the triboelectric series briefly come in contact with each other. The triboelectric series arranges materials by their readiness to give away or take electrons.

Some common materials that readily donate electrons include leather, human hair, and paper. Some common materials that readily accept electrons include wood, Teflon, and gold. When the donor material and the acceptor material come in contact, temporary electrochemical bonds are formed between the two [15]. These bonds provide the pathway for the donor material to send electrons to the acceptor material. Since this happens almost instantaneously, triboelectric nano-generators theoretically have no minimum or maximum operating frequency. When the two

materials are separated, the donor material has fewer electrons than usual, which results in a net positive charge. The acceptor material, on the other hand, has a net negative charge [16]. Because one material has a net negative charge and one has a net positive charge, there is a charge imbalance between the two [17]. If the two materials are connected via a wire while they are still separated, the charge imbalance will cause the extra electrons from the acceptor material to flow back to the donor material. This flow of electrons is considered the electric current. This cycle is repeated when the donor and acceptor materials come in contact again. The full process is depicted in Figure 1:

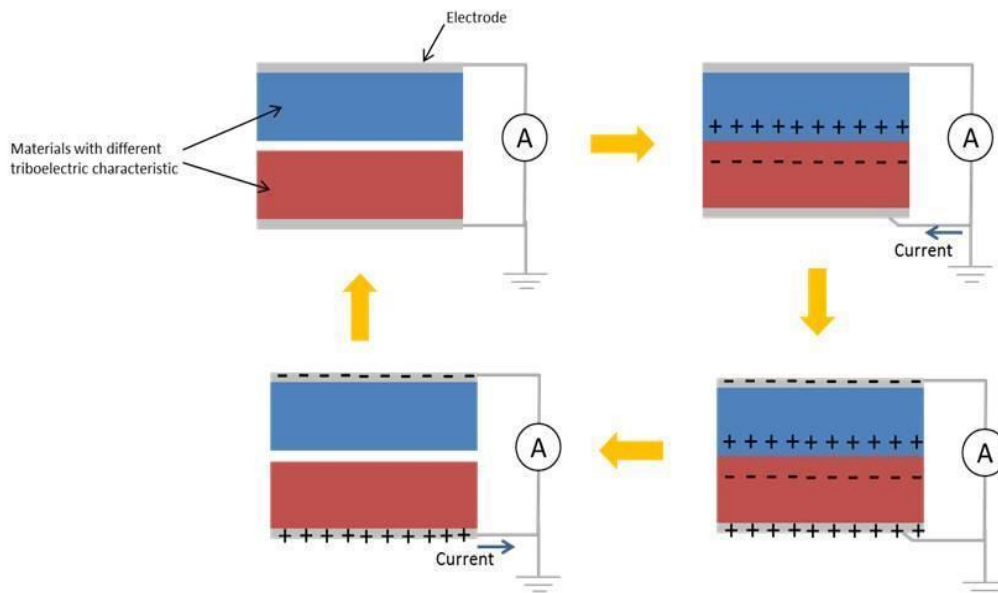


Figure 1: The Triboelectric Process [40]

The ideal triboelectric nano-generator involves using materials from opposite ends of the triboelectric series, such as Teflon and leather. Controllable factors that can affect a triboelectric nano-generator include the distance of separation as well as the surface area of the material [18]. The first triboelectric nano-generator journal was published in 2012 [19]. Since triboelectric nano-generators were discovered so recently, there have not been many prototypes developed or practical applications suggested.

Electromagnetic

Another method to harvest energy is using electromagnetic generators. This method harvests energy via an electric conductor moving through a magnetic field, which creates a potential difference and therefore can produce an electric current [4]. The electrical conductor in most cases is usually a coil that turns due to an external force. This magnetic field is a result of a permanent magnet in the system, as seen in Figure 2. The electrons are free to flow when the coil moves between the poles of the permanent magnet.

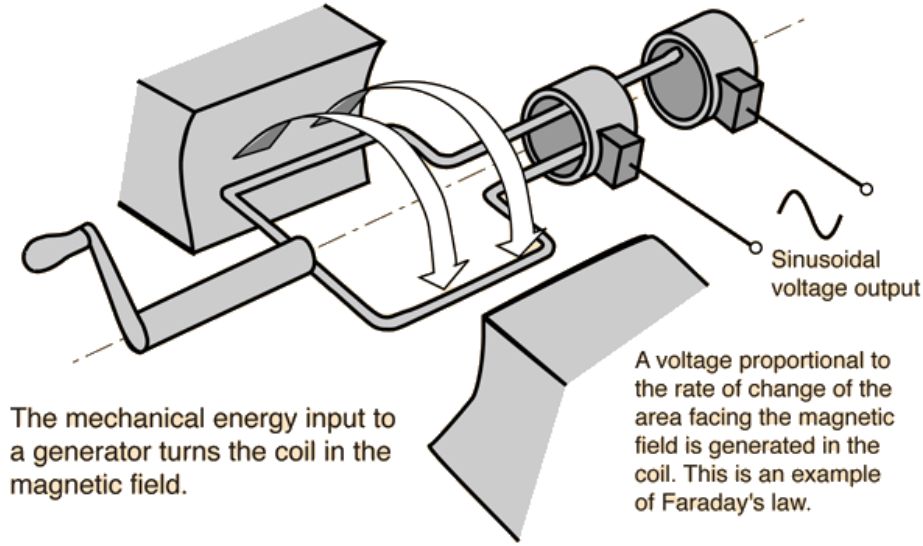


Figure 2: Electromagnetic Generator Schematic [41]

This type of electrical power generation is based on Faraday's law of electromagnetic induction. Faraday recognized the direct relationship for the number of coil turns to the voltage output of the generator [4]. Equation 9 demonstrates how the product of the number of turns (N) and the time-based derivative of the flux linkage (ϕ) creates voltage (V). As the number of turns increases, the voltage output along with the resistance of the coil increases. As long as the device is aligned in the same axis as the force turning the coil, this generator can efficiently create electrical power [20].

$$V = -N(d\phi / dt) \quad (\text{eq.9})$$

The voltage that is extracted from the electromagnetic generator connects the coil terminals to a resistance and allows a current to flow through the coil. This current produces a magnetic field which acts to oppose the electromagnetic field. The interaction between the two fields creates a force which opposes the electromagnetic force, F_{em} , which is when the mechanical energy is transformed into electrical energy [4]. This F_{em} force is directly proportional to the current that is induced as well as the electromagnetic damping, D_{em} as shown in Equation 10 below.

$$F_{em} = D_{em}(dx/dt) \quad (\text{eq.10})$$

In an experimental study by Vinod Challa, it was found that piezoelectric generators has a higher energy density than electromagnetic generators in small scale application. Challa's electromagnetic generator measured a $6.9 \mu\text{W cm}^{-3}$ power density, while the piezoelectric generator measured a power density of $9.1 \mu\text{W cm}^{-3}$ for small scale applications, where power output is in milli/microwatt range [21]. From these results, vibration energy harvesters will be best served by piezoelectric and electrostatic transduction rather than electromagnetic generators.

Electromagnetic generators are capable of producing larger amounts of power in the kilowatt range when used in larger scale applications [4].

Piezoelectric

First discovered in the mid-1800s but not fully understood and explained until 1880 by Jacques and Pierre Curie, the piezoelectric effect is a property of certain crystalline materials [22]. The most common material is quartz [23]. This effect has two variations, direct and inverse. The direct piezoelectric effect involves a change in electric potential due to an applied mechanical stress while the inverse effect involves the opposite, a material deformation due to applied electric field [24]. Piezoelectricity is becoming more popular as the need for renewable energy increases.

Certain materials have this piezoelectric property due to a large amount of dipoles within their structures. A dipole occurs in molecules when there is an unequal distribution of charge due to concentrations of electrons. One side of the structure will have a partially positive charge, while the other side will have a partially negative charge [25]. In addition, dipoles have an inherent direction and when dipoles are near each other they align to have the same direction. When the materials are placed under mechanical stress it affects the crystalline structure of the material molecules causing groups of dipoles to align, giving the material a polarity, otherwise known as a specific negative or positive alignment. As more stress is applied, dipoles become displaced, which results in more electricity being generated [25]. Hence, the change in electric potential is directly proportional to the amount of applied mechanical stress. It has also been shown that compression outputs a voltage with the same charge polarity as the material while tension outputs one with the opposite polarity [24]. Figure 3 shows the direct piezoelectric effect:

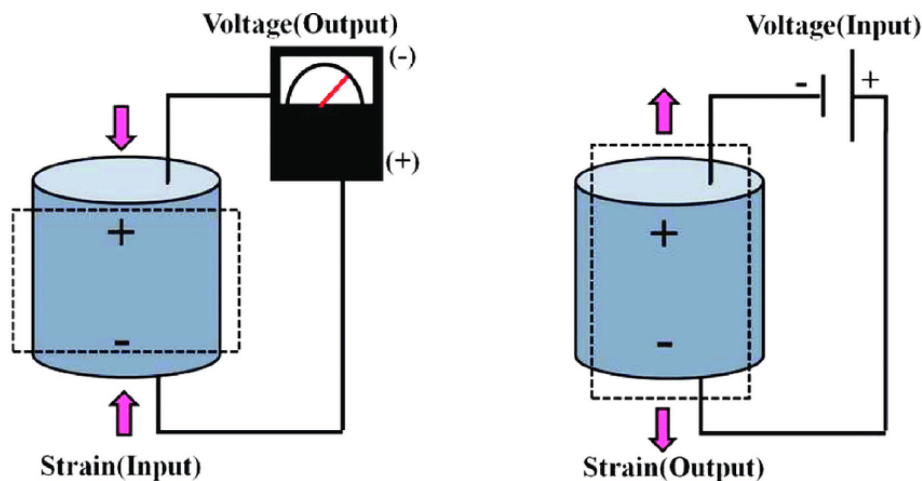


Figure 3: Direct and Converse Piezoelectric Effect [65]

The electrical displacement and electric field vectors of the piezoelectric materials can be found from the stress and strain charge as shown in equations 11-14 below [26]. Equation 11 depicts

the strain vector (S) as equivalent to the compliance matrix (sE) times the stress vector (T) plus the piezoelectric coupling matrix in strain charge (d) times multiplied with time (t) and the electric field vector (E). Equation 12 depicts the electrical displacement (D) as the piezoelectric coupling matrix in strain charge times the stress vector plus the strain (ϵ) multiplied with the stress vector and the electric field vector. Equation 13 depicts the stress vector as the stiffness matrix (cE) times the strain vector minus the piezoelectric coupling matrix in stress charge (e) multiplied with time and the electric field vector. Equation 14 depicts the electrical displacement as the piezoelectric coupling matrix in stress charge times the electric permittivity (s) plus the strain multiplied with the strain vector and the electric field vector.

Strain Charge:

$$S = [sE]T + [dt]E \quad (\text{eq.11})$$

$$D = [d]T + [\epsilon T]E \quad (\text{eq.12})$$

Stress Charge:

$$T = [cE]S - [et]E \quad (\text{eq.13})$$

$$D = [e]s + [\epsilon S]E \quad (\text{eq.14})$$

Since its discovery, the piezoelectric effect has been studied and applied to thousands of applications ranging from military sonar, artificial organs, and to energy harvesters embedded in a shoe heel. One of the reasons that piezoelectric material can be used in so many different ways is due to the variety of materials that have been found, or made to have this effect. While naturally occurring materials are still used quite often, a group of manufactured materials called piezo-ceramics have been shown to have a high material dielectric and stiffness allowing them to have a higher output of electricity while being able to handle heavy loads. However, piezo-ceramics have low durability [27]. Researchers have been trying to improve the efficiency of piezoelectric materials. Not only are researchers trying to create new materials entirely, but they are also looking for new ways to arrange the piezoelectric materials and their circuitry. For example, it has been shown that stacking piezoelectric crystals leads to an overall higher voltage output.

In the case of the mechanical deformation of vibrations, different piezoelectric materials react to different rates of deformation based on the amount of strain experienced. It is important to choose the correct piezoelectric material for the chosen application so as to have the highest efficiency output. When designing a piezoelectric energy harvester, the size of the device and material must be considered. There are micro and macro scale applications. Micro-scale generators are small enough to be incorporated into microelectronic systems but experience low power output. In comparison to the micro-scale generators, macro-scale generators are capable of producing a larger power output, but are limited to applications based on the larger size. The piezoelectric material is chosen based on the application it will be used in. Materials range from very flexible to being very stiff and fragile. The tradeoff between these two extremes is that the stiffer the material is, the higher the strain coefficient is for the piezoelectric material [28].

Piezoelectric Circuitry

The electrical potential that is produced by a piezoelectric device is in the form of an alternating current (AC). In order to collect and store this energy, the AC signals must be converted to direct current (DC) signals using a diode rectifier. Diodes limit the current to flow in only one direction [38]. Diodes also have a turn-on voltage, which is a small amount of voltage that is required in order for the diode to conduct. In the case of power diodes, the forward voltage is around 0.2-0.3 volts. When a diode is applied to an AC signal, conduction of the signal is only allowed for the upper bound. Figure 4 depicts what happens to the signal as it crosses through a diode.



Figure 4: Signal Response from a Diode [38]

Diodes can be used in many different arrangements in a circuit to produce slightly different results. Half-wave rectifiers are the simplest of the circuits, but smoothing of the signal is not as effective when compared to the full wave rectifier circuit, which uses two diodes. These diodes are used for both alternating directions of the input signal. As the input current flows, the diodes in the half wave rectifier circuit alternate in supplying to the load.

The Full Wave Bridge Rectifier is a common circuit that is used in power rectification. This circuit uses four diodes in a bridge arrangement, which contains two pairs of diodes. The diodes are arranged in series. As a result, current will flow through two diodes, creating two voltage drops while the ripple frequency doubles to twice the amount of the input frequency. After the bridge, a capacitor can be used to smooth out the fluctuations in the DC output voltage signal. Figure 5 depicts the Full Wave Bridge Rectifier Circuit with a smoothing capacitor.

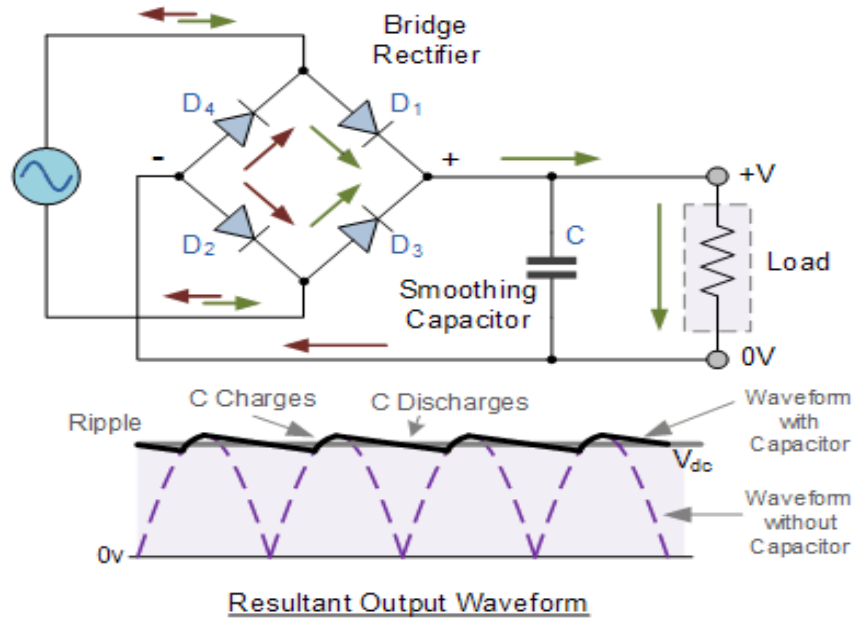


Figure 5: Full Wave Bridge Rectifier Circuit [39]

Methods of Vibration Transference in a Piezoelectric Setup

In past studies, piezoelectric materials have used cantilever beams as a way to transfer the frequency of the external vibration so that the piezoelectric material experiences the maximum amount of strain. Cantilever beams are able to create a resonant frequency because only one end of the beam is fixed. As a load is applied anywhere near the free side, the beam will deflect accordingly. This phenomenon can be explained by the inertia of the beam once the initial force that displaces the beam is removed [29]. Assuming the beam consists of a uniform cross-sectional area, the maximum deflection can be calculated at the end of the beam as shown in Equation 15 below [30].

$$\delta = \left(\frac{Fa^3}{3EI} \right) \left(\frac{1+3b}{2a} \right) \quad (\text{eq.15})$$

In Equation 15 above, δ represents the maximum deflection at the end of the cantilever beam. E is the modulus of elasticity of the material and can be found in a properties table. I is the moment of Inertia. b is the location where the force vector is applied. The variable a represents the distance between where the beam is fixed and where the force vector (F) can be drawn.

The deflection of the beam affects how the piezoelectric material experiences strain along the beam. This calculation can be used to understand the placement of the piezoelectric material as well as what sort of dimensions might be required of the cantilever beam in order to achieve a certain deflection.

Cantilever beams are often used as the mechanical intermediate from the external vibrations to the piezoelectric material. The downside of using a cantilever beam structure is that some of the external energy is lost to damping. One application for piezoelectric materials on a cantilever beam comes from a US Patent granted back in 2008. This patent shows a device that is a self-sustaining vibration sensor. A piezoelectric ceramic layer was placed on top of a non-piezoelectric layer in the shape of a cantilever beam. The non-piezoelectric layer is longer and thicker than the piezoelectric layer, so it acts as a proof mass. The beam uses the output from the piezoelectric layer to both determine the vibration being experienced by the structure and also power that sensor [31].

Past Research Applications using Piezoelectric Systems

There have been many proofs of concepts and prototypes that harness piezoelectric material to produce electricity. As the need for more innovative sources of reusable energy continues to rise, there are more efforts being made to research and develop applications for piezoelectric materials.

In one study, researchers from the University of Notre Dame and Seoul National University developed an energy harvesting skin using piezoelectricity. The energy harvesting skin consists of thin patches of lead zirconate titanate, a high-efficiency piezoelectric material. This structure was directly attached and shaped to fit the vibrating surface of the condensing unit within an outdoor air conditioning unit. This system produced an average of 3.7mW [32].

One set of researchers developed an energy harvesting floor tile that uses piezoelectric cantilevers. The frequency of the vibrations of human footsteps is raised through a combination of springs and permanent magnets. The higher frequency vibrations allow the piezoelectric to draw more energy than would be obtained from the natural frequency of a human footfall. This study concluded that a possible application was these tiles sustainably supporting low-power electronics [33].

There are also applications for piezoelectric systems to be used in bridges. One article discusses the concept of generating electric power from a piezoelectric-wafer-equipped bridge. The goal was to support essential bridge systems such as sensors and lighting; however the electrical output was low. They incorporated the piezo in the bridge bearings. They spent approximately \$5,000 for wiring, adhesives, instrumentations, etc. They experienced short-circuiting in all of the 0.0105-inch thick wafers and were unable to gather energy from them. They suggest installing the wafers on both sides of the shim so they would share a common ground and thus be connected electrically in series, which would raise the current generated [34].

In another article, various applications of piezoelectric technology in urban settings are analyzed. One of the proposed scenarios is “implementing a piezo power-generating device along high traffic pedestrian’s pathways in the City of Melbourne (Australia), evaluating real-time and storage options, considering harvesting the energy during the day and using it at night time when

needed.” Also, the author mentions that most piezoelectric applications usually have a small power generation. They also state how companies such as Pavegen and Japon are using electromagnetic and piezoelectric technologies but are not publishing much about their processes or what they are doing with the energy that is being generated [35].

Issues with current harvesting methods and applications

Finding and optimizing new and innovative methods for harvesting energy comes with many challenges. For many types of energy harvesting, conversion efficiency is the main problem. Often energy dissipates during collection and by the time it is processed into a usable form there is less than what the systems actually produce. In addition, many of these energy harvesting methods do not produce enough to save an amount of money to offset their costs.

For vibrations in particular, a pressing challenge is frequency. Current methods for harvesting the energy rely on tuning springs, piezoelectric materials, or other forms to the specific frequency of the device being used. This limits not only the materials that an energy harvester can use, but also the applications that a specific harvester may be applied to. Another concern with frequency is if the resonant frequency matches that of the natural frequency. When this occurs, the amplitude of the frequencies is greatly increased, which puts the system at risk for failure [36].

Some disadvantages of vibrations include the risk of damaging the equipment as well as reducing the productivity and lifespan. Unwanted vibrations waste energy and can also damage the floor beneath the machine [43]. Mounts have been developed along with bedding systems, such as machine pads to dampen shock and vibration that machines experience during dynamic loads. Mounts help isolate the machine from the factory floor and provide leveling. The rubber material that is used to dampen can be made with various geometries and hardness to accommodate specific applications [42].

The transmission of shock and vibrations can be reduced up to 90% when machines are suspended on components that absorb energy [44]. These components are composed of resilient material such as neoprene, fiberglass, springs, and various mounts. Within various mounts, isolators are used to absorb energy from vibrations. Spring isolators are recommended for use with compressors, pumps, and fans. Air isolation mounts are recommended for use with mechanical equipment and equipment that is very sensitive to surrounding vibrations [45].

In one experimental study, a tuned mass damper (TMD) was developed to reduce machine vibrations. The TMD is composed of variable masses attached to a spring and dashpot. These components are arranged in parallel to allow the vertical vibrational energy to dissipate through the dashpot. Results showed a reduction in acceleration by 41-56% when tested with the floor and a 90% reduction when tested with beams [46].

Methodology

Design Specifications

To create a product that can harvest energy as well as dampen vibrations from a machine, the following design specifications were outlined.

- Minimum dimensions must be able to accommodate machine base/leg
- Piezoelectric as the energy harvesting material
- Electrically insulated material for the base
- Must accommodate for highest measured deflection point
- Ability to be connected to identical units
- Must be durable enough to withstand repeated loading
- Must damp some vibrations from the machine to improve machine life

The design specifications were chosen with the consumer and product life cycle in mind. The dimensions of one prototype unit were chosen to accommodate the size of a household blender. Testing with a blender was chosen as it allows for a small testing and storage environment while also being portable. In addition, the information gathered from the prototype can be scaled up to larger applications. Selection of the piezoelectric material as the energy harvesting method was based on detailed background research.

Preliminary Analysis

Tachometer Testing

The motor speed and the acceleration of the body of the blender were tested to see if there was any correlation.

The five advertised motor settings of the blender were measured using a tachometer. The data was recorded and averaged for each of the settings and the results are depicted in Table 1. The complete test procedure for obtaining the following results as well as the complete data obtained can be found in Appendix A.

Table 1: Tachometer Results for each Speed

	Average RPM	Standard Deviation
Chop	18469	175.45
Mix	18705	1654.8
Grate	19763	369.43
Blend	20530	428.59
Liquify	20172	138.94

It was determined from testing that the average motor speed for each of the settings gradually increases. Ranked from slowest to fastest, the settings are chop, mix, grate, blend, and then liquefy. The data in the table is listed in revolutions per minute. The minimum and maximum values from the data table averages are 17,766 RPM (296 Hz) and 21,174 RPM (353 Hz), respectively. To obtain the frequency and acceleration of the housing of the blender, an accelerometer was attached at various locations and data was collected.

Preliminary Accelerometer Testing

A LabVIEW program was used in conjunction with multiple accelerometers to record acceleration and to calculate the frequencies of the blender. The first accelerometer used aided in the initial design of the LabVIEW program and processed data for 1 axis of the accelerometer at a time. In order to improve this process, a 3-axis ADXL356C accelerometer by Analog Devices was used. This accelerometer was wired to measure data in the analog mode (X_{out} , Y_{out} , and Z_{out} pins) along with the 40g range. Due to a suspected voltage spike in the accelerometer, data from these tests were disregarded and a third and final accelerometer was used, the ADXL326Z accelerometer.

The LabVIEW program received data in the form of voltage readings from a data acquisition box (DAQ) which was wired to the accelerometer. The voltage readings were calibrated by subtracting the local mean from each reading. In this case, the local mean refers to the mean of the data points that are slightly before and after the point being analyzed. The calibrated value was then divided by the sensitivity of the accelerometer, which is in units of mV/g where g is gravity. The acceleration values were then measured over time and the LabVIEW recorded all data in an excel file for later use. The experimental wiring setup for accelerometer one is shown in Figure 6.

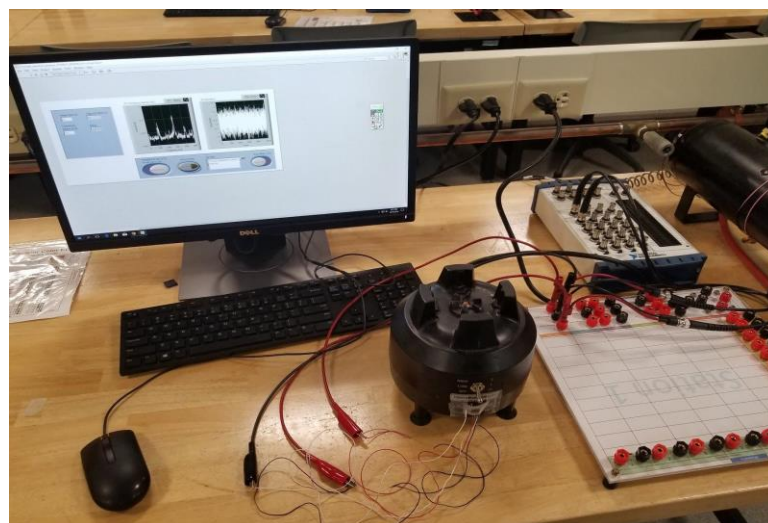


Figure 6: Initial Experiment Wiring Setup

The second accelerometer required modification to the initial LabVIEW program to allow multiple signal inputs from each axis. Testing revealed that LabVIEW has only one internal clock, and therefore only one axis could be read at a time. Instead of reading all 3 axes simultaneously, a stacked sequence structure was used in the LabVIEW program to read each axis sequentially. The program was designed to record the X-Axis data for two seconds, the Y-Axis data for two seconds, and then the Z-Axis data for two seconds. Readings from the Z-axis were constantly switching between 2g and 10g at unusually long intervals. The inconsistent data that was collected led to the conclusion the accelerometer was damaged from an excitation voltage that exceeded what the sensor was capable of handling. Thus, a new accelerometer was used to collect data, which is described further in the next section.

Final Accelerometer Testing

The third and final accelerometer that was used to measure the acceleration of the blender was a 3-axis analog devices accelerometer connected to an evaluation board (EVAL-ADXL326Z). This third accelerometer was purchased with a pre-soldered evaluation board to make soldering the wires and handling the very small sensor easier. In addition, the spaces for the capacitors on the board allowed for the elimination of the external capacitor circuit for filtering. It was found when testing the board that the capacitors were in fact not needed, but it was a consideration during the decision to purchase this board. The schematic is depicted below in Figure 7. In order to prevent a recurrence of running too much voltage through the sensor, when using the third accelerometer (the ADXL326) the input voltage was given from 2 AA batteries.

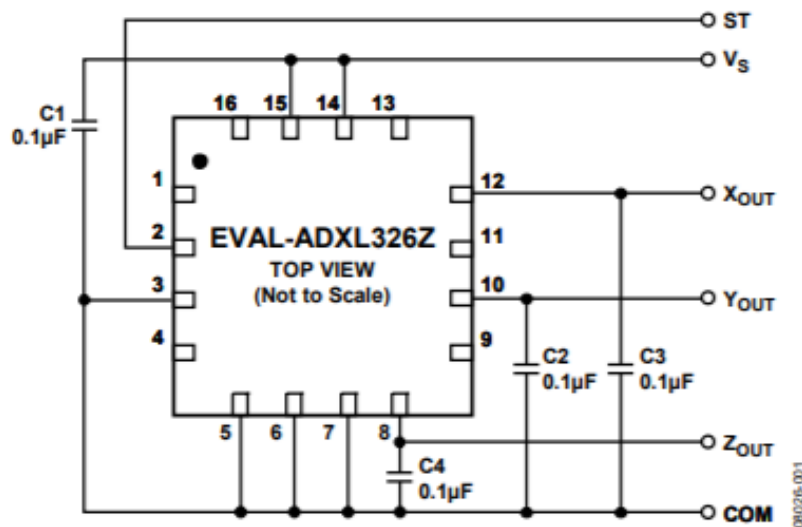


Figure 7: Pin Schematic of Evaluation Board with ADXL326 Accelerometer [66]

The evaluation board and attached accelerometer were wired differentially to a data acquisition box (DAQ). Due to the differential wiring, the LabVIEW program was altered to read the voltage difference between the two wires to determine the acceleration. In order to simplify the

wiring process, only one axis was read at a time. The wiring configuration can be seen below in Figure 8. The LabVIEW program took the acceleration and using the fast Fourier transform (FFT), plotted the frequencies seen in peak form. A screenshot of the LabVIEW showing the acceleration over one second and subsequent FFT graph can be seen below in Figure 9.

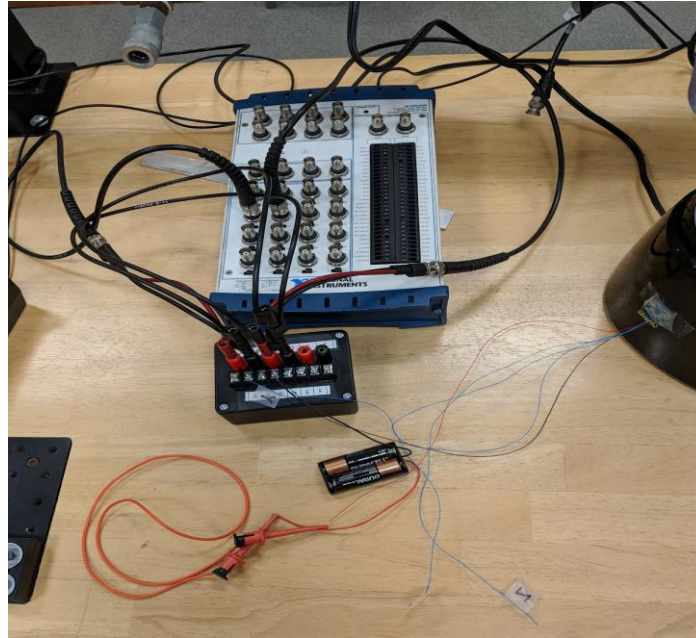


Figure 8: Wiring Configuration of EVAL-ADXL326Z to DAQ Unit with AA Battery Input Voltage

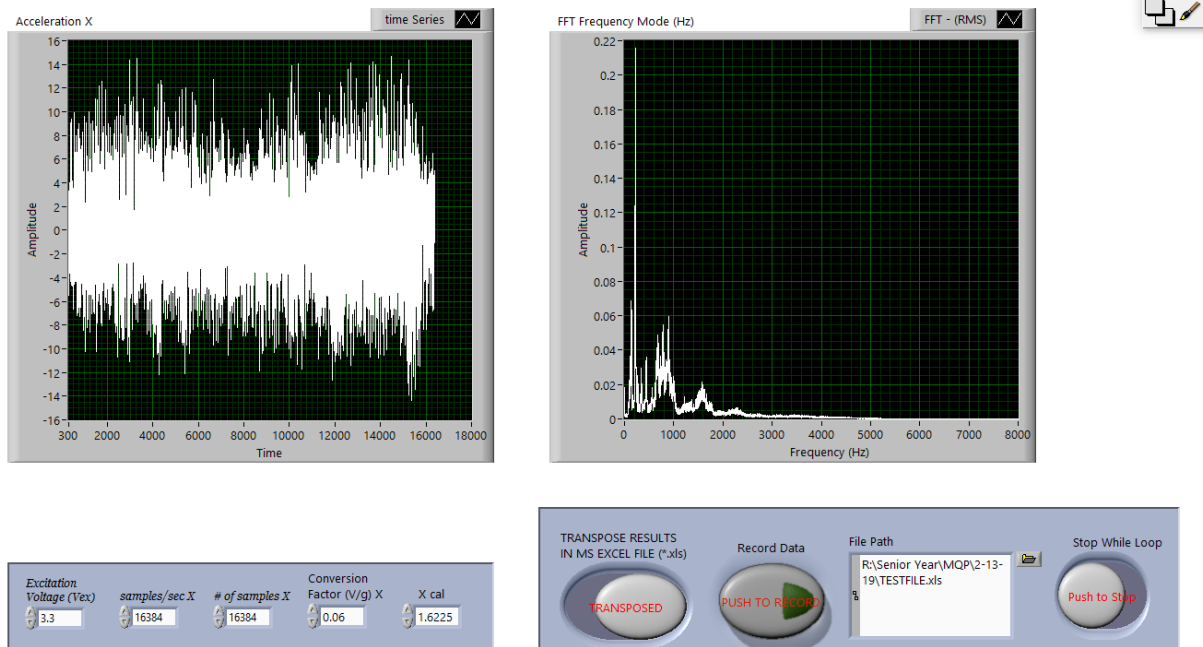


Figure 9: Screenshot of LabVIEW Program (Cornstarch, Liquify Speed, Z-Axis, Trial 1)

Variables that were tested, included all 3 axes, placement of the accelerometer, all 5 blender settings, and 2 different liquid viscosities (cornstarch mixed with water (at a 1:3 ratio) and just water). The axes for this accelerometer is shown in Figure 10:

AXES OF ACCELERATION SENSITIVITY

Figure 60 shows the axes of acceleration sensitivity. Note that the output voltage increases when accelerated along the sensitive axis.

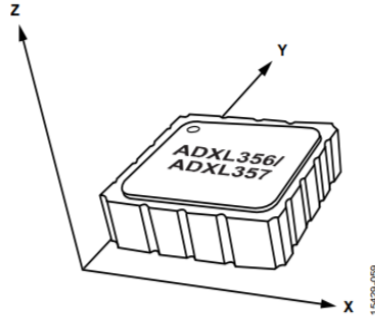


Figure 10: Accelerometer Axis Orientation

The two different positions the accelerometer was tested on the blender are depicted below in Figures 11 and 12.

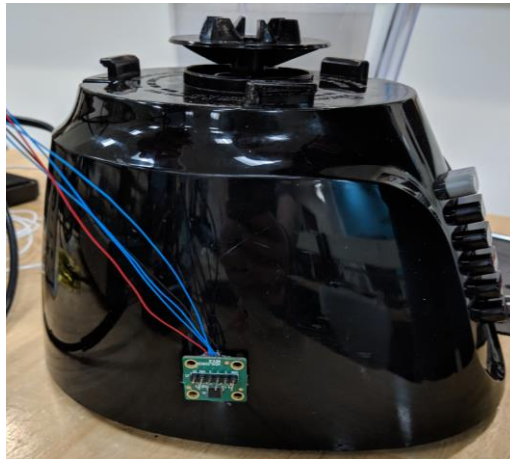


Figure 11: Position 1



Figure 12: Position 2

For each test, 10 seconds of data were recorded. The excel file containing the acceleration for those 10 seconds was then averaged using the root mean square (RMS) method. The full testing procedures can be found in Appendix B. Table 2 below shows an example of one of the tables containing the root mean square acceleration data.

Table 2: Sample RMS Average of Acceleration (g)

Chop (5sec)	RPM			Mix (5sec)	RPM			Grate (5sec)	RPM		
Blender Speed	Max	Min	Final	Blender Speed	Max	Min	Final	Blender Speed	Max	Min	Final
<i>Trial 1</i>	18699	18154	18266	<i>Trial 1</i>	21939	18889	18946	<i>Trial 1</i>	21091	19376	19449
<i>Trial 2</i>	19356	18091	18329	<i>Trial 2</i>	19002	12878	19002	<i>Trial 2</i>	19542	19192	19526
<i>Trial 3</i>	18883	18244	18335	<i>Trial 3</i>	18963	18939	18939	<i>Trial 3</i>	19473	19382	19473
<i>Trial 4</i>	18372	18248	18356	<i>Trial 4</i>	19157	19059	19059	<i>Trial 4</i>	20583	19410	19500
<i>Trial 5</i>	18425	18214	18264	<i>Trial 5</i>	19152	19068	19092	<i>Trial 5</i>	20226	19351	19351
Average	18747	18190	18310	Average	19643	17767	19008	Average	20183	19342	19460
Blend (5sec)	RPM			Liquify (5sec)	RPM			Pulse (*)	RPM		
Blender Speed	Max	Min	Final	Blender Speed	Max	Min	Final	Blender Speed	Max	Min	Final
<i>Trial 1</i>	21411	19869	19976	<i>Trial 1</i>	20813	20003	20146	<i>Trial 1</i>	9347.0	88.400	3131.0
<i>Trial 2</i>	21603	19942	20011	<i>Trial 2</i>	20185	20029	20161	<i>Trial 2</i>	9736.0	6742.0	6742.0
<i>Trial 3</i>	22193	19902	20010	<i>Trial 3</i>	20099	19992	20099	<i>Trial 3</i>	6468.0	396.90	3700.0
<i>Trial 4</i>	20496	19890	20029	<i>Trial 4</i>	20183	20091	20183	<i>Trial 4</i>	10734	7893.0	7893.0
<i>Trial 5</i>	20168	19829	19995	<i>Trial 5</i>	20244	20083	20203	<i>Trial 5</i>	10850	8280.0	8280.0
Average	21174	19886	20004	Average	20305	20040	20158	Average	9427.0	4680.1	5949.2

Deflection values were calculated from the acceleration data that had been collected. The data was first processed over time (t) by taking one peak in the acceleration graph and finding the area (A) underneath it using the trapezoidal method to find velocity. This was then repeated to find deflection. The equation for the trapezoidal method is shown in Equation 16.

$$A = \frac{1}{2}(f(t_2) - f(t_1))\left(\frac{1}{t_2 - t_1}\right) \quad (\text{eq.16})$$

Multiple peaks were analyzed from separate acceleration graphs and then averaged to get a mean deflection of 5 micrometers. The five trials can be seen in Table 3. The typical sensitivity of the

accelerometer is 57 mV/g and the bias level was calibrated for each axis at approximately 1.5 V. Reference Appendix B for a more detailed calibration procedure. Depending on the specific stack, piezoelectric materials meet the needs of this design criterion with a deflection range of 3.3-100 micrometers. Table 4 below shows the type of piezoelectric stacks and chips offered from Thorlabs [58].

Table 3: Deflection Values

Trial #	Deflection:
Trial 1	4.78
Trial 2	6.09
Trial 3	5.14
Trial 4	5.99
Trial 5	5.18
Average	5.44
Standard Deviation	0.574

Table 4: Piezoelectric Materials Deflection Ranges

Piezo-ceramic	Deflection Range
Discrete Piezoelectric Stacks	5.2 μm to 100.0 μm Travel
Co-Fired Piezoelectric Actuators	4.6 μm to 17.4 μm Travel
Round Piezoelectric Actuators	3.3 μm to 12.0 μm Travel
Low-Voltage Piezoelectric Chips	0.7 μm to 3.6 μm Travel

Considering the maximum deflection calculated, Co-Fired Piezoelectric Actuators were determined to have the best performance for the project. Co-Fired Piezoelectric stacks act as one unit, rather than multiple chips acting individually. According to Thorlabs, “These co-fired stacks are able to achieve a free stroke displacement that is significantly larger than their single-chip counterparts” [59]. Specifically, part # AE0505D08F was selected and the specification sheet is located in Appendix D.

This information contributed to the decision to purchase actuator stacks with a deflection range of 9.1 micrometers. After purchasing the piezoelectric materials it was found that the error in the accelerometer data made it very difficult to get clean integrations. The error in each reading, which was accumulated during the integration over the 16,384 readings per second, created a drift in the results. To try to remedy this the acceleration was integrated over smaller time

periods: about 1 millisecond at a time. An example deflection curve can be seen below in Figure 13. It can be seen that there is a peak change of approximately 15 micrometers. Due to time constraints the piezoelectric components could not be replaced, but it was determined that they would still work in the operating range; they would just not deflect the possible maximum.

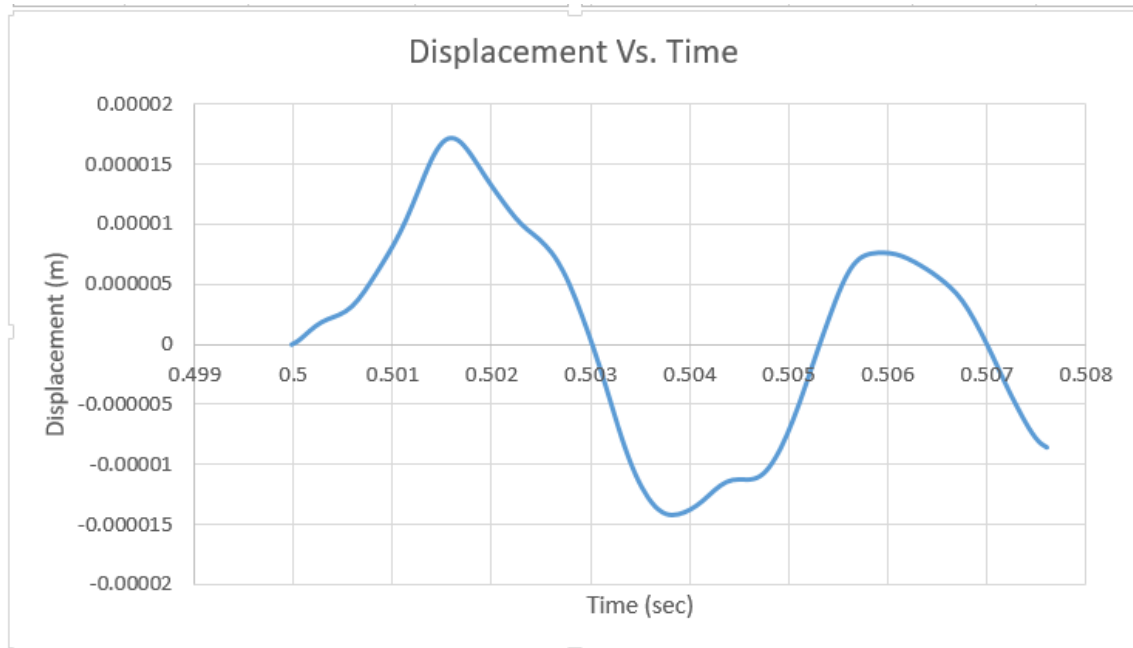


Figure 13: Sample Displacement Curve (Cornstarch, Liquefy Speed, Z-Axis, Trial 1)

The peak deflection value can then be used in Equation 17 below, to determine an appropriate spring constant (k).

$$F = kx = ma \quad (\text{eq.17})$$

The spring force (F) is defined as the spring constant (k) times the deflection (x). By Newton's second law this was set equal to the mass (m) times the acceleration (a). Equation 17 was used with the averaged values from testing. The blender's liquefy setting was used for all analysis and prototype testing because the preliminary testing revealed that it had the largest acceleration and deflection. The deflection value used was 15 micrometers because as seen in Figure 13, it was a representative of the peak displacement. The acceleration value was averaged over the cornstarch, liquefy trials and found to be about 4 g, and the mass was estimated to be 0.1 kg. With these variables, the spring constant (k -value) needed was found to be on the order of 10^3 [lbs/in]. Due to size constraints (0.5 inches in length) with the prototype and the availability of such a high k -value (8,403 lb/in), the appropriate spring could not be purchased. Instead, the highest k -value spring available (395 lbs/in) was used.

The frequency data collected was used to identify a peak frequency where the majority of the accelerations occur. A sample frequency graph can be seen pictured below in Figure 14.

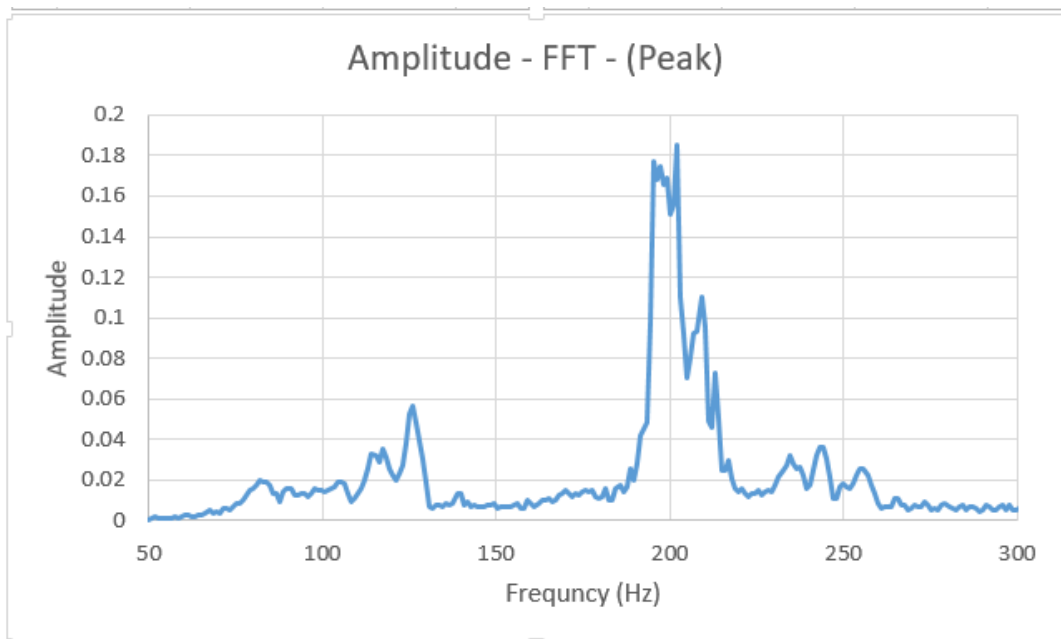


Figure 14: Sample Frequency FFT Graph (Cornstarch, Liquify Speed, Z-Axis, Trial 1)

From the cornstarch and water graphs the peak frequencies were determined to be around 200 Hz and 225 Hz, respectfully. When purchasing the piezoelectric materials, actuators that worked at these frequencies or multiples of these frequencies were avoided in order to avoid having the actuators hit resonance.

Design

Prototype One

The aim of constructing the first prototype was to identify initial manufacturing and design challenges.

The prototype casing and blender support pad were 3D printed out of PLA (polylactic acid) plastic filament using the printers in the WPI Foisie Innovation Studio. Due to the limited size of the 3D printing plate, the dimensions of the inner casing were 10.5" x 10.5" x 2.5" with a quarter inch thickness. The support pad dimensions were 8.25" x 8.25" x 0.50" to be large enough to fit the blender. The manufacturing method of 3D printing was an advantageous decision for the initial prototype due to the low-cost of PLA and the team's accessibility to the printer.

Five ball bearing transfer units were used to support the blender pad while limiting friction. They were attached to the base with simple screws as pictured in Figure 15. Four small temporary cardboard standoffs were taped to the bottom of the base to allow space to secure the screws.



Figure 15: Base box with Ball Bearing Transfer Units

A sample spring was taped to the side of the blender support pad as a placeholder as accelerometer testing had yet to be completed and so the needed spring constants were still unknown. However, the spring was not stiff enough and would bend sideways, putting no pressure on the piezoelectric. It was hypothesized that the actual springs with their higher spring constant would not perform this way.

One piezoelectric element was placed on the inside of the casing at the same height as the spring using double sided sticky tape. In order for the spring to be properly secured to the prototype, small pieces of cardboard were taped to it. The cardboard, however, did not stay connected well and was also not stiff. The entire prototype one can be seen pictured below in Figure 16:

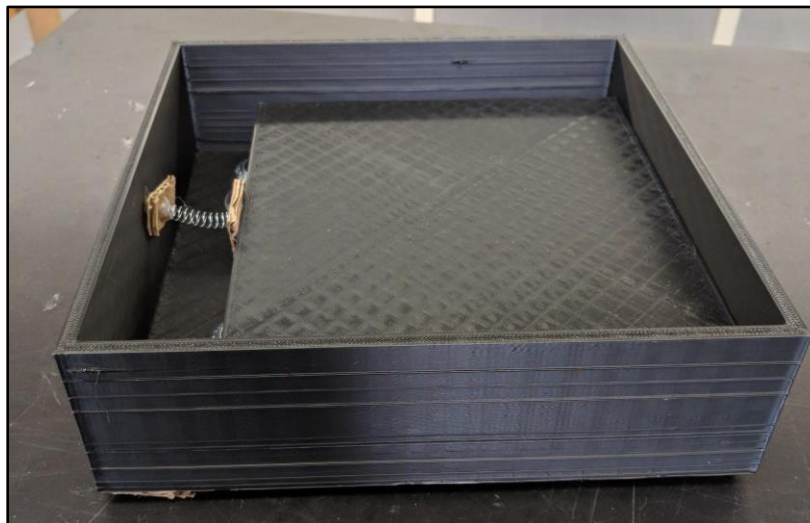


Figure 16: Prototype One

Prototype one revealed the need for several design modifications. Modifications to the casing involved changing the material for visual effects and adding an additional casing layer to contain

the circuitry. Also, the springs should have closed and grounded ends to better adhere to the prototype.

Prototype Two

Prototype two addresses the design modifications that were considered after the construction of prototype one.

The base for the prototype was expanded and made hollow. The new dimensions of the inner layer were 10" x 10.5" x 2.25". 3D printing the base for the second prototype was not a viable option as the expanded base was now too large for the available printers. Instead, acrylic was chosen as the base material for its durability, compatibility with the available machinery, high availability and inexpensiveness, and transparency to allow the circuit to be monitored whilst inside the base. Quarter inch acrylic sheets were cut into pieces and then cemented together to create the hollow base which protected the circuitry from unnecessary movement and harm. The outer dimensions were 12"x 12"x 3.5".

The blender support pad stayed the same as the one used in prototype one since there were no issues found with it during prototype one testing. In addition, the springs and ball bearings from prototype one were reused as information from the preliminary testing had yet to be analyzed and no changes seemed evident.

All four piezoelectric elements were integrated into the base of the second prototype. Small holes were drilled in the inner casing later to allow for the wires of the elements to be connected to the circuit. The piezoelectric materials were held in place just above the holes using double sided sticky tape.

The second prototype contained a completely connected testing circuit as pictured in Figure 17 below. The circuit consisted of the four piezoelectric elements, each wired to a diode rectifier that transforms the alternating current produced by the piezoelectric materials to a direct current. The current can then be measured and stored as seen in Figure 17. The four elements and their corresponding rectifiers are wired in parallel. A study in Malaysia showed that using multiple piezoelectric elements in a parallel wiring scheme had not only a higher power conversion efficiency, but also a faster charging time [60]. In addition, due to the parallel wiring, if one element were to break or falter, energy would still be obtained from the other three elements. If the piezoelectric materials were wired in series, then an issue with one would cause the whole system to fail. The parallel wiring also connects the piezoelectric materials to a capacitor. The capacitor serves to further smooth out any ripples providing a smoother current.

CAD drawings of the conceptual prototype two can be seen in Figures 18 and 19. The actual prototype two is shown in Figure 20. Additionally, the circuit diagram for prototype two can be seen below in Figure 21.

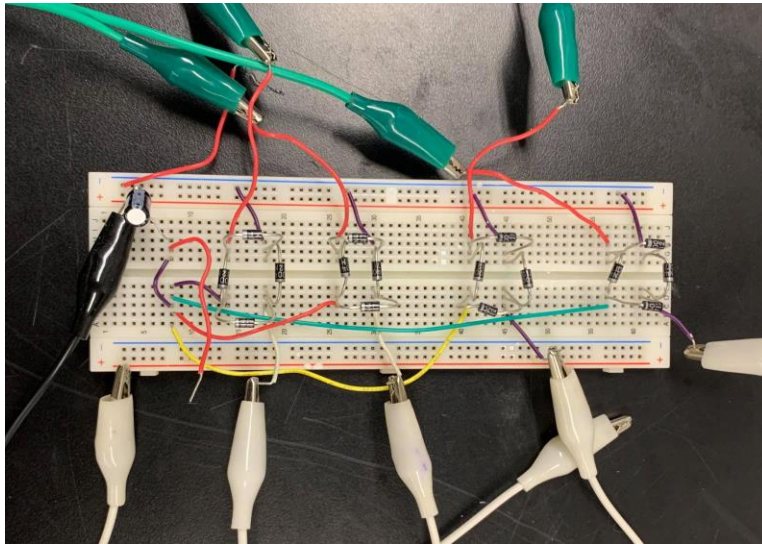


Figure 17: Energy Harvesting Circuit

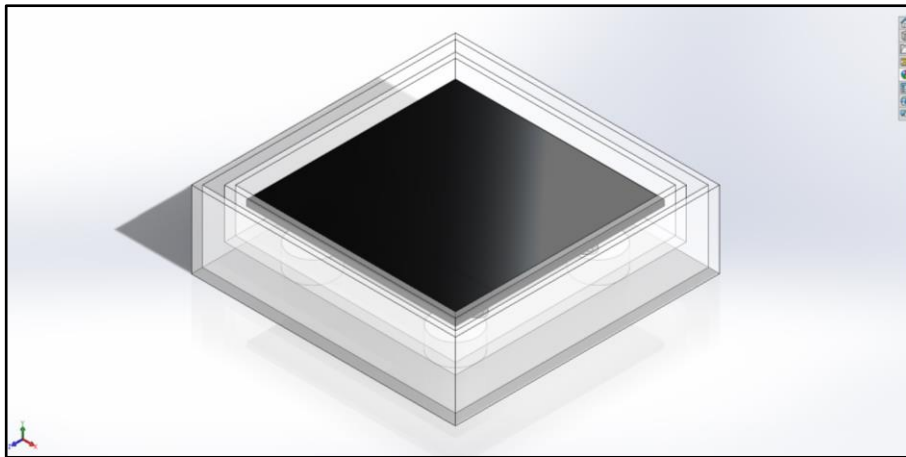


Figure 18: Isometric View of CAD drawing of Prototype Two

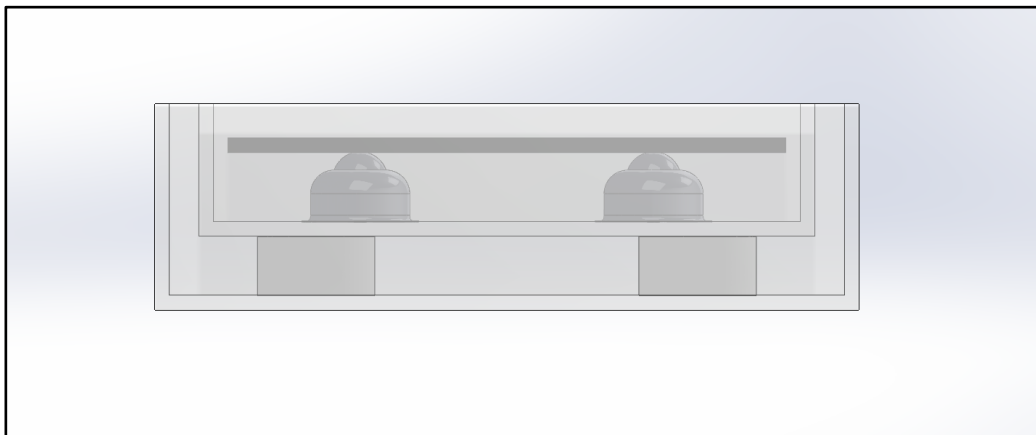


Figure 19: Side View of the CAD drawing of Prototype Two

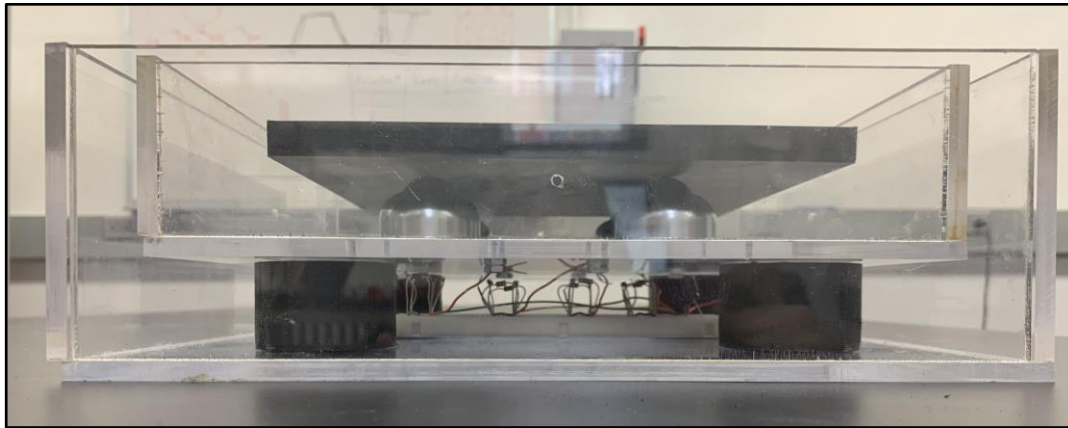


Figure 20: Photo of Prototype Two

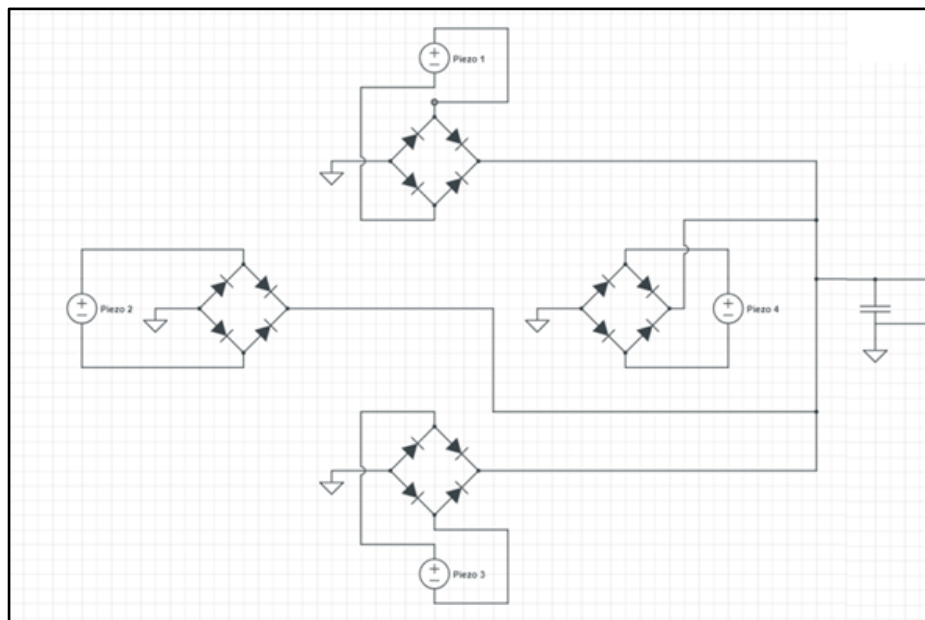


Figure 21: Prototype Two Circuit Diagram

Prototype Three

The third prototype has the same casing as prototype two, but with some added features that help protect the piezoelectric stacks. Testing prototype two showed that the piezoelectric stacks were not fully secure and could be damaged easily if misaligned. Round sleeves were designed and 3D printed to hold the piezo in place, and attach to the inside casing walls. After the new springs were ordered, the blender support pad dimensions had to be changed to accommodate for their size. Since the piezoelectric stacks needed to be in compression, the pad had to have precise dimensions, therefore it was laser cut out of plywood instead of 3D printed. Laser cutting was also cheaper and quicker than 3D printing the plate. The final support pad dimensions were 8" x 7.9375" x 0.25". Small acrylic spring pads were again hot glued to the springs to provide more

surface area. The final assembly can be seen in Figure 22 below and the damping subsystem can be seen up close in Figure 23.

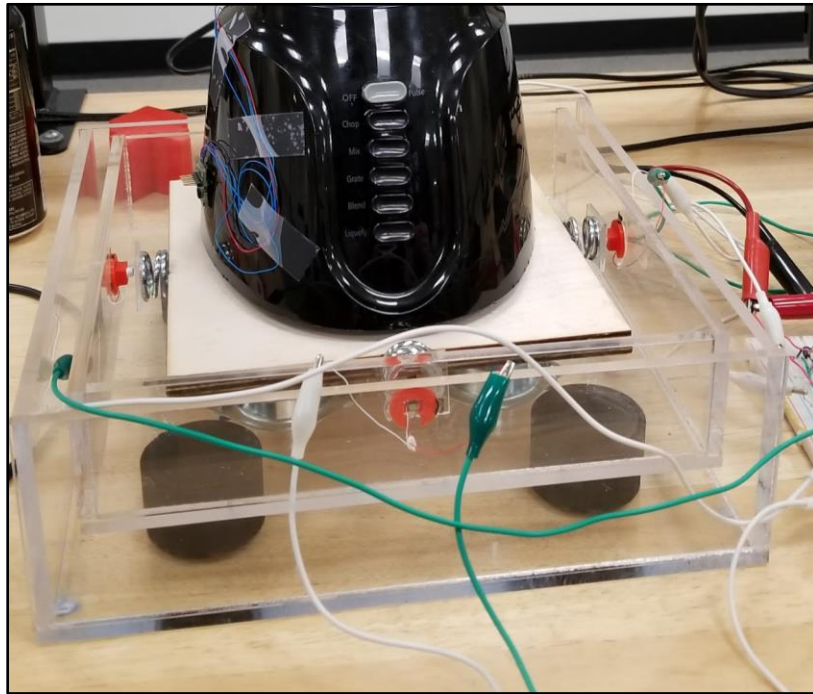


Figure 22: Prototype Three with the circuit outside for testing purposes

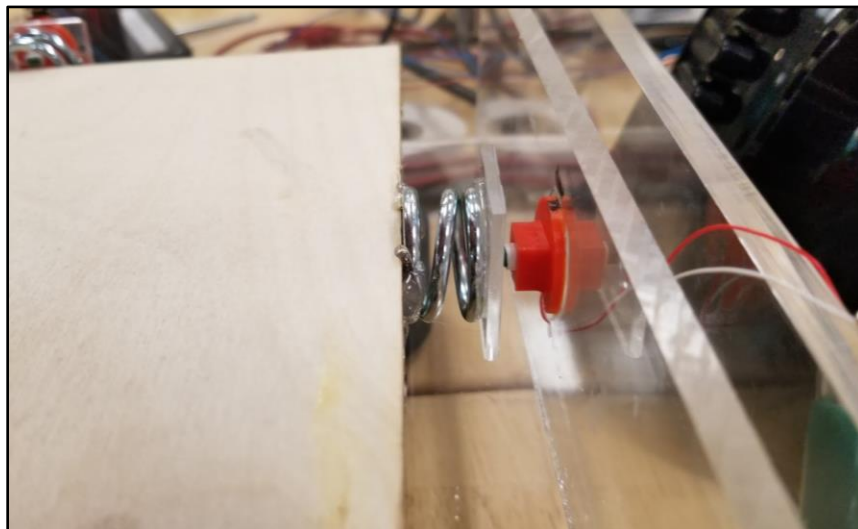


Figure 23: Close-up of piezoelectric stack, spring, and plate assembly (Damping Subsystem)

Results

Prototype three was determined to be viable and was tested while measuring both acceleration and voltage output. It was first tested with its springs. The decision was then made to remove the springs and retest the prototype to determine damping. The blender's liquefy setting was used for all tests because the preliminary testing revealed that it had the largest acceleration and deflection. Reference Appendix C for the complete test procedure.

Spring Incorporated Version

Three trials were taken with both water and cornstarch in the blender and averaged. Figures 24 and 26 below depicts the acceleration and Figures 25 and 27 depicts the voltage that were recorded simultaneously for one trial. The capacitor was manually discharged through short-circuiting prior to the LabVIEW program running in an attempt to start the voltage graphs at a voltage of zero. However, if there was any delay between the manual discharge and the start of the data recording, it was possible for excess charge remaining in the piezoelectric materials from previous tests to leak into the capacitor. This would cause the voltage to be higher than zero when the recording started. This error can be seen in the voltage graphs shown below in Figures 25 and 27.

The acceleration graph shows only the first 1000 samples (less than 1 second of data) to give a clearer view of what the signal looked like. However, the RMS value was calculated using the full ten seconds of data samples. The RMS value for both water and cornstarch testing was 4.52g. The voltage rate over the capacitor (slope of the data in Figures 25 and 27) for the water and cornstarch trials are similar with rates of 5.8×10^{-4} V/s and 4.5×10^{-4} V/s, respectively. The R^2 value for Figure 25 is 0.965. Since this value is close to 1.0, the linear trend line shown accurately represents the data. This is true for all of the voltage vs time graphs.

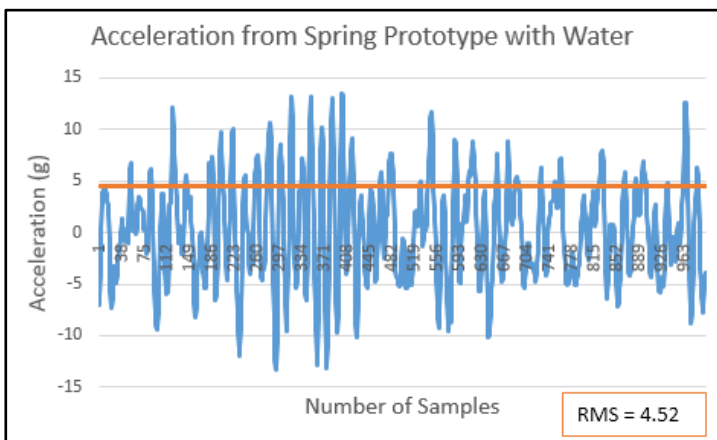


Figure 24: Spring Prototype Water Acceleration Graph

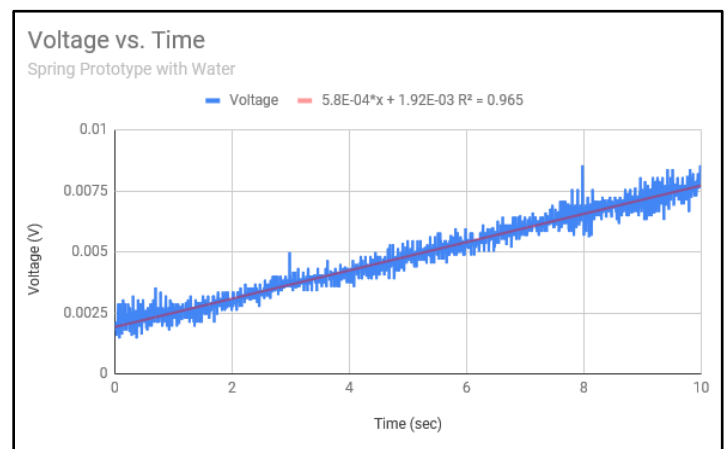


Figure 25: Spring Prototype Water Voltage Graph

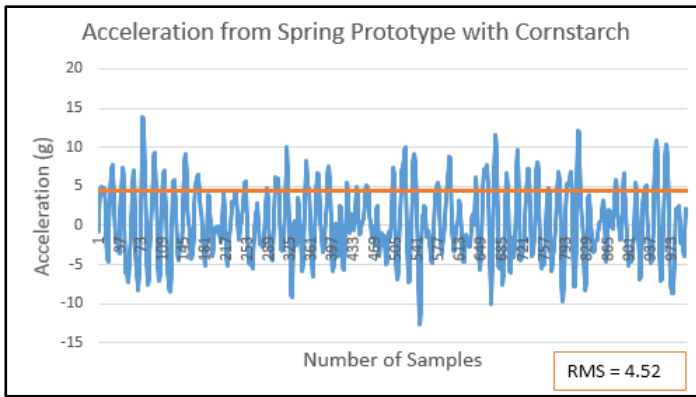


Figure 26: Spring Prototype Cornstarch Acceleration Graph

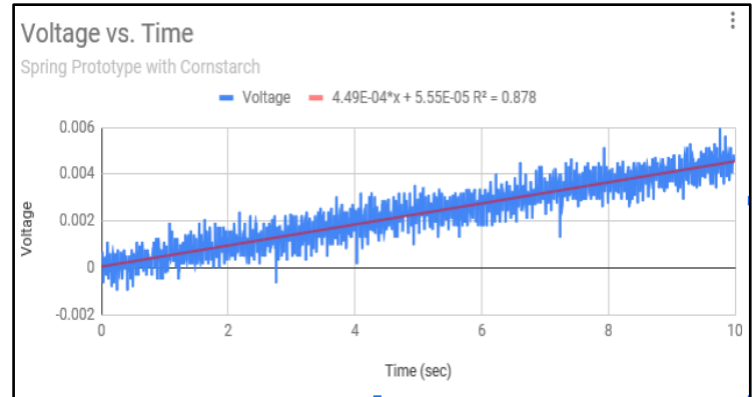


Figure 27: Spring Prototype Cornstarch Voltage Graph

Spring-less Version

Data collected from the spring-less version are shown below in Figures 28-31. The spring-less version was tested with the same procedure as the one with springs. The acceleration RMS value for water is 4.49g. The RMS value for Cornstarch is slightly higher with a value of 4.91g. A possible reason for this slight variance is that cornstarch is a non-Newtonian fluid. Twenty tablespoons of cornstarch were added to the cornstarch mixture, which is about 0.15kg heavier than just the water mixture. The height of the fluid surface in the cornstarch mixture had 5 more ounces of liquid than the height of just the water trials. The voltage rate over the capacitor for the water and cornstarch trials are again similar with rates of $1.57 \times 10^{-3} \text{ V/s}$ and $1.45 \times 10^{-3} \text{ V/s}$, respectively.

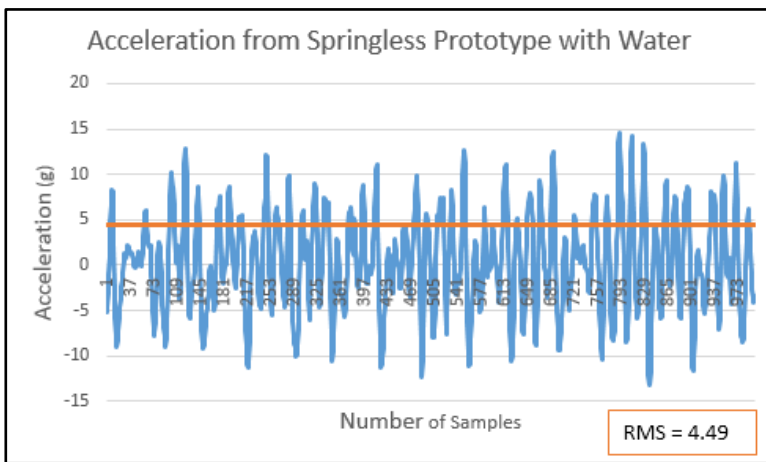


Figure 28: Spring-less Prototype Water Acceleration Graph

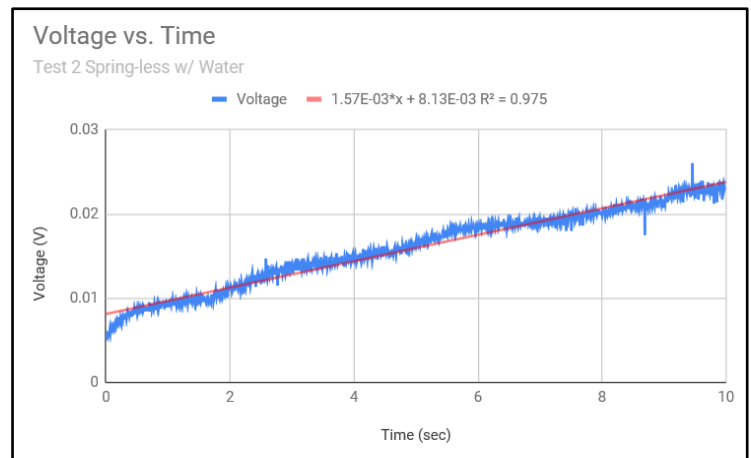


Figure 29: Spring-less Prototype Water Voltage Graph

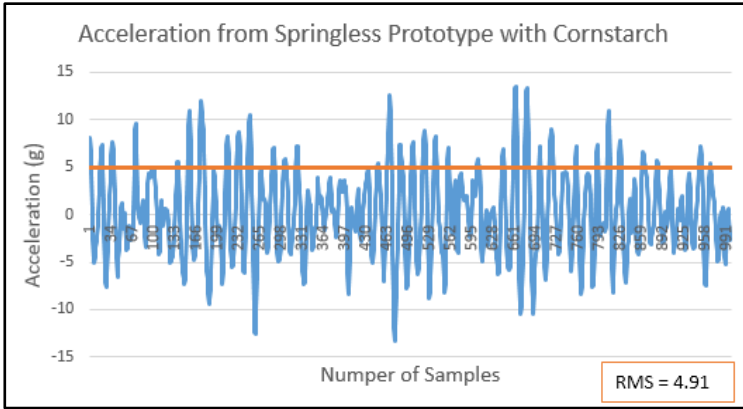


Figure 30: Spring-less Prototype Cornstarch Acceleration Graph

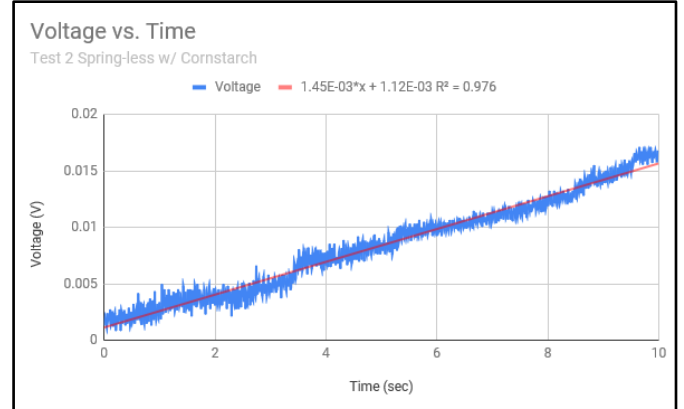


Figure 31: Spring-less Prototype Cornstarch Voltage Graph

Power Output

From the voltage recordings power (P) was calculated using the equations below. The capacitor value (C) that was used in the circuit is 100×10^{-6} F. This is multiplied by the difference in voltage (v) squared to calculate the amount of energy (E) produced as is seen in Equation 18. This energy divided by the time (t) over which the prototype was run gives power output of the prototype as is seen in Equation 19.

$$E = \frac{1}{2} C(v_2^2 - v_1^2) \quad (\text{eq.18})$$

$$P = \frac{E}{t} \quad (\text{eq.19})$$

Tables 5 and 6 depicts all the trials with the average for each.

Table 5: Spring-less Power Output

Trial #	Min Voltage (V₁)	Max Voltage (V₂)	Energy (J)	Time (s)	Power (W)
Cornstarch					
1	0.00193	0.0130	8.30×10^{-9}	9.98	8.30×10^{-10}
2	0.00112	0.0156	1.21×10^{-8}	9.98	1.21×10^{-9}
3	-0.0000852	0.0117	6.84×10^{-9}	9.98	6.84×10^{-10}
Average					9.09×10^{-10}
Water					
1	0.00290	0.0197	1.89×10^{-8}	9.98	1.90×10^{-9}
2	0.00813	0.0238	2.51×10^{-8}	9.98	2.51×10^{-9}
3	0.00807	0.0257	2.97×10^{-8}	9.98	2.97×10^{-9}
Average					2.46×10^{-9}

Table 6: Springs Incorporated Power Output

Trial #	Min Voltage (V₁)	Max Voltage (V₂)	Energy (J)	Time (s)	Power (W)
Cornstarch					
1	-0.0000840	0.00447	1.00 X 10 ⁻⁹	9.98	1.00 X 10 ⁻¹⁰
2	0.0000555	0.00455	1.03 X 10 ⁻⁹	9.98	1.03 X 10 ⁻¹⁰
3	0.000650	0.00491	1.18 X 10 ⁻⁹	9.98	1.18 X 10 ⁻¹⁰
Average					1.07 X 10 ⁻¹⁰
Water					
1	0.00176	0.00727	2.49X 10 ⁻⁹	9.98	2.49X 10 ⁻¹⁰
2	0.00192	0.00772	2.80X 10 ⁻⁹	9.98	2.80X 10 ⁻¹⁰
3	0.00154	0.00737	2.60X 10 ⁻⁹	9.98	2.60X 10 ⁻¹⁰
Average					2.62X 10 ⁻¹⁰

Conclusion

Table 7: Testing Overview

Prototype, Liquid Trial	RMS Acceleration Average	RMS Acceleration Standard Deviation	Power Average	Power Standard Deviation
Spring, Water	4.47 g	0.0800 g	2.62×10^{-10} W	1.57×10^{-11} W
Spring, Cornstarch	4.55 g	0.0800 g	1.07×10^{-10} W	9.64×10^{-12} W
Spring-less, Water	4.44 g	0.0600 g	2.46×10^{-9} W	5.36×10^{-10} W
Spring-less, Cornstarch	4.89 g	0.0624 g	9.09×10^{-10} W	2.21×10^{-10} W

From the data collected, as shown in Table 7 above, there are some key takeaways that illustrate the effectiveness of the device. When comparing the two systems, the spring-less system has a higher power output in both the cornstarch and water trials. This is also present in the water trials where the spring-less system exhibited a higher power average output than the spring system. From this, it is clear that the spring-less system is the better design in terms of power output. However, there is a tradeoff. Although the spring-less system generates more power, there is less damping. Damping increases the lifespan of the blender overtime because it decreases the amount of vibration the blender is subjected to, thus putting less stress on the machinery.

The RMS acceleration values from the cornstarch acceleration experiments show that the spring system has a lower value than the system without springs. The RMS acceleration value for the water trials are nearly unchanged. A possible explanation is because cornstarch is a non-Newtonian fluid and is therefore more prone to experiencing uneven loads. Both the piezoelectric and springs dampen the machine vibrations, so without them the acceleration values would be much higher. The preferred choice for an energy harvester would be a unit without springs, but a unit that both dampens and harvests energy is the overall better choice when considering the lifespan of the machines. As such the spring incorporated version is recommended.

When looking at the entire design and testing process, there are a few improvements that could be made when building this prototype for future applications. This design was meant to both harvest energy and dampen the vibrations of the source, whether that is a blender or another machine. In order to dampen the amount of vibrations to a specific amount, springs are needed with a specific k-value. The k-value calculated to significantly dampen the vibrations based on

the acceleration of the blender was 8,403 lb/in. However, the design of the prototype prohibited the purchase of the proper k-value since there was only a clearance of a ½” between the plate and the piezo-ceramic. The highest k-value at a ½” clearance was 395 lb/in. This spring only provides partial dampening; therefore, the design must be larger to incorporate a higher k-value spring.

Manufacturing Considerations

Previous to this section, the prototype built and tested was specific to one application: the household blender. In order to expand the prototype to be used in various applications in the market, several design considerations need to be taken into account to ensure success in its mass production. There are two different types of components used in the creation of this vibration harvester. There are ordered parts and 3D printed parts that were used when creating this prototype. The materials list is shown below in Table 8.

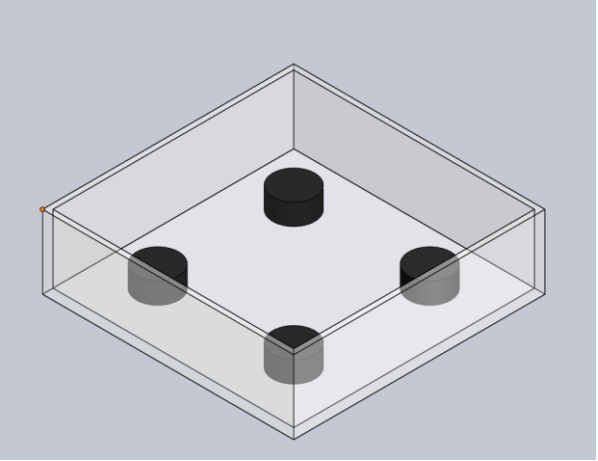
Table 8: Bill of Materials

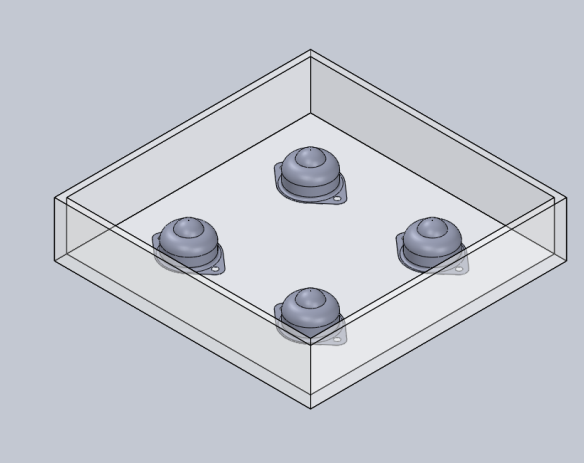
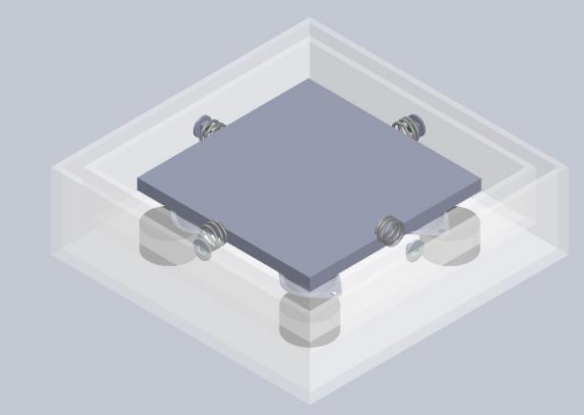
Material	Quantity/Size	Vendor	Cost
Piezoelectric Actuators	4	ThorLabs	\$342.48
Acrylic Sheets	2	Acrylic	\$59.54
Acrylic Cement	1	MSC	\$18.44
Ball Bearings	4	MSC	\$15.50
Wiring	X	WPI	N/A
Blender	1	Walmart	\$15.85
Free-moving base	1 (PLA)	3D Printed	N/A
Standoffs	4	3D Printed	N/A
Springs	12	MSC	\$25.00
Total Cost	N/A	N/A	\$476.81

*Note that costs would decrease when mass manufactured due to volume

The as-is process to assemble the vibration harvester prototype using the bill of materials is listed below. This process is mostly conducted manually with no automation and with theoretical calculations. The assembly process to create the vibrations harvester can be automated in certain sections and can reduce the overall lead time.

Assembly Procedure

<p><u>Acrylic Cutting: 30 minutes</u></p> <ol style="list-style-type: none">1. Laser Cut Acrylic<ol style="list-style-type: none">a. Outer Case (12"x 12")<ol style="list-style-type: none">i. Outer Walls (12"x3.5"), (11.5" x 3.5")b. Inner Case (10.5"x 10.5")<ol style="list-style-type: none">i. Inner walls (10" x 2.25"), (10.5" x 2.25") <p><u>3D Printing Procedures: 10 hours</u></p> <ol style="list-style-type: none">1. Sent Solidworks file of support pad to 3D printer2. Sent Solidworks file of standoffs to 3D printer <p><u>Outer Base Assembly: 3.5 hours</u></p> <ol style="list-style-type: none">1. Cement edges together of outer case1. Sit and cure for 72 hours to increase tensile strength of the hold2. Epoxy 2" in diameter 1.25" in height standoffs	
--	---

<p><u>Inner Base Assembly:</u></p> <ol style="list-style-type: none"> 1. Measured and Drilled holes for ball bearings for the inner case: 2. 4 through holes inner wall 1” from the bottom of the inner wall 3. Screw in 4 ball bearings 	
<p><u>Piezoelectric Stacks/Chips Attachment:</u> <u>30 minutes</u></p> <ol style="list-style-type: none"> 1. Epoxy the lead side of the piezoelectric actuator to the inner wall above the drilled holes 2. Epoxy 3D printed piezoelectric supports 	

Total Approximate Production Time: 14.5 Hours

Automating and Improving the As-Is Process

Automation is advantageous in assembly this product because it will help reduce the time and cost it takes to create each product. In the prototype initially developed, acrylic was laser cut and assembled by hand for the casing. Without automation, the risk of user error increases with the amount of time required to assemble the pieces. The acrylic sheets can be laser cut by ABB powered robotic arms that use code to cut the acrylic with precision [48]. Although there would be a learning curve to learn the technology, the overall takt time of the production process would decrease. Therefore, once the acrylic is laser cut, glue/cement dispensing robots can be used to immediately attach together cement directly on the edges and place them with appropriate walls and cases. This automated process can reduce up to 1 hour of manually cementing the individual pieces together, which is how long it took when assembling the prototype. A 3-axis CNC machine can be used to drill holes in the acrylic with proper dimensioning.

The most time consuming manufacturing process is the 3D printing of the standoffs and the moving support pad in separate assembly line. Instead of 3D printing these parts, they can be injection molded using via steel tooling as that would save labor cost and time and material cost. Since this would be an on-demand manufacturing production line, mold prices would be low and part prices would be high. However, since the parts are single cavity molds, the production price of 1,000 units would not exceed \$2,500 [53]. This would be cost effective compared to 3D printing these parts where the cost of 3D printing 1,000 units would be approximately \$11,000 of material cost.

By applying lean manufacturing principles, these assembly lines can be automated to take the injection molds of steel and insert them directly into the acrylic structure via manually or a robotic arm.

Energy Analysis and Application

Since the power of the system is calculated to be 1.2×10^{-10} W, there are few applications that this product can power. Many piezoelectric systems look at MEMS (Microelectromechanical Systems) as a viable application. The energy provided by this unit is not adequate to power these devices as they need an average of 2-10V and 100mA to operate [55]. However, the power generated from the prototype would be suitable for NEMS (Nanoelectromechanical Systems). These systems are miniaturized versions of MEMS to the point where they are a couple of hundred nanometers large. The applications for these devices include sensors, medical diagnostics, displays, and data storage [56]. As the market for these devices continues to grow, the need for small energy sources also increases. Many of the NEMS devices require a power source of at least 10 atto-watts, which is 1×10^{-18} W. This unit would be capable of powering any number of these devices based on the power output from the prototype.

The footprint of the prototype is 1 ft^2 or approximately 0.093 m^2 . Taking the largest power produced by the prototype with the damping subsystem as 2.62×10^{-10} W, the power density is calculated to be $2.82 \times 10^{-9} \text{ W/m}^2$. This power output is too small to power anything larger than a NEMS. The power output produced by the prototype is expected to change when different vibration sources are used. Different vibration sources would have different magnitudes of acceleration. Testing revealed that as the magnitude of accelerations increased, so did the amount of power output by the prototype. Therefore, when the prototype is used on other vibration sources, such as a CNC machine, the power output and hence power density will likely be higher than what the blender produced. In addition, storing the energy in a larger capacitor or a battery would increase the power density allowing for more applications.

Expanded Manufacturing Applications

As seen in other applications, there is an option for a commercial version of this design. Funding for such a device is one of the primary issues when it comes to reusable energy applications. Companies such as Pavegen have utilized human motion to create a floor that that can generate electricity. With funding from the London Business Angels, a private investment firm, Pavegen was able to maintain a firm financial footing [49]. Today, their clients include Nike, Google and Siemens [50]. In the case of this energy harvester, there are applications for manufacturing companies that would be interested in purchasing this device as a dampener/harvester for the machining floor.

Other than funding, there would have to be design changes that would change as well. In a manufacturing floor setting, there would have to be a materials change for the outer and inner base since CNC machines are much heavier than blenders. As stated above, the preferred materials would be a metal that can resist a high compressive stress. For this, steel is recommended due to its high elastic modulus and cheap cost. However, in order for the piezoelectric circuit not to interact with the steel, the steel sheet would have to be insulated by rubber along with the standoffs.

The last aspect of this system that would need to be expanded is the piezoelectric circuit. Since the as-is system uses 4 parallel circuits with four diode rectifiers and a single capacitor, the circuit would have to be expanded in order to make a harvester/dampener for a CNC machining floor. In order to make a larger power bank, the circuit must be modified by creating printed circuit board that would be individual applied for each energy harvesting tile. Financially, buying them in bulks of thousands is feasible rather than purchasing equipment to manufacture the boards. These PCB's can be bought offshores in bulk quantity by many Chinese manufacturers with all the required components such as diodes and capacitors in the PCB. One such company is Elecrow who can manufacture 1,000 units approximately for \$2,500 [57].

While only one energy harvesting pad was created for prototyping, the pad was designed to be able to be wired to other pads as a PCB model and be placed under larger machinery. The pads would work together to create a floor for the machines to be placed upon. A potential area where this could be very useful would be in a manufacturing plant where there are hundreds of machines that are constantly running and producing vibrations. The pads would harvest the energy and store it in batteries for further use.

An example PCB circuit of three tiles wired together is shown below in Figure 32. Each tile is shown to be wired to a DC smoothing capacitor and then in parallel to a charge controller. The tiles are wired in parallel so that if one tile fails the other tiles will still be able to provide energy to the system. A battery and a system of lights are also shown wired to the charge controller.

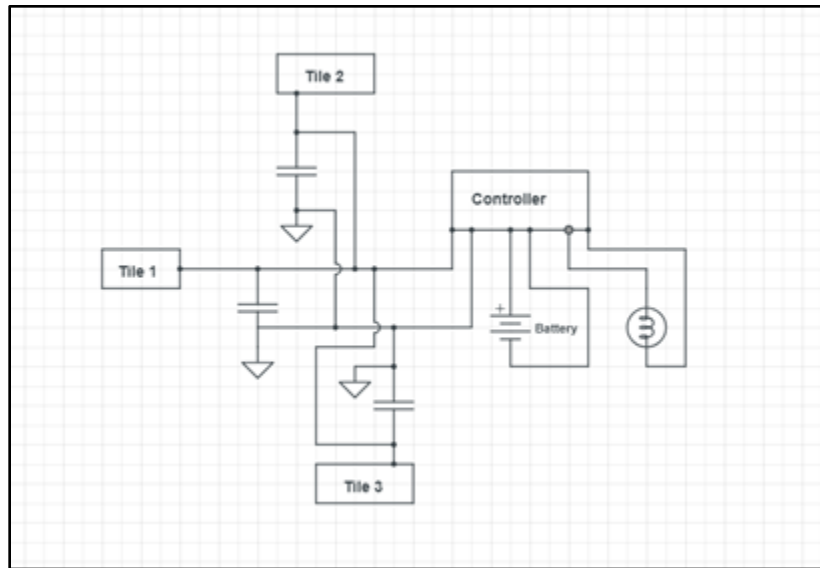


Figure 32: Proposed Circuit for Multiple Tile Platform

Charge controllers take the incoming voltage and current from the energy harvesting system, in this case the piezoelectric tiles, and manipulate them to be constant. The controller then allocates a certain amount of energy to the load, for example, a light system and to the battery. If there is excess energy it will store it in the battery, then if there is ever a time where the harvesting system is not providing enough energy to power the load, the controller will tell the battery to provide the needed energy. Charge controllers contain all the internal circuitry required to provide just the right amount of current and voltage to charge the battery. The type of charge controller needed depends on both the battery and the incoming energy. Many types of batteries, such as lithium ion require certain phases of both constant current and voltage to safely charge and store energy. Certain controllers are programmed to handle different battery types. The controller also must be chosen based on the amount of incoming energy as both controllers and batteries will have a range of safe voltages and current under which they can operate since the output voltage values need to be tested.

Impact

Advancements in modern technology allow for further use and development of machine automation. The efficiency of machines is affected by many factors, including energy lost through vibrations. Studies have shown that harvesting vibrational energy through the use of piezoelectric materials generally outputs more power per area than other methods of harvesting energy [61]. The amount of power output per piezo is on the scale of microwatts and milli-watts [62] [63].

Currently, piezoelectric materials are being used as an alternative method to power low energy devices, such as wireless sensors. Advantages of using this alternative method include the potential cost benefit from annual maintenance and replacement of batteries.

The project aims to expand the use of piezoelectric harvesting devices to larger applications, as well as making it adaptable for various uses on both household and commercial levels. The prototype is designed for use on a small scale, specifically a household blender. The data collected from the small-scale design is used to theoretically scale the prototype to meet the needs of commercial use, such as a factory floor. Each unit prototype can be made as connectable tiles to allow user flexibility in fitting a certain amount of units for a particular application.

Another part of the prototype design involved damping the system vibrations through the use of springs and partly through the use of piezoelectric material. Damping of system vibrations typically increases the longevity of the product because the risk of damage and fatigue are reduced.

A major limitation encountered in this project was not having the resources to test the design on a larger scale application. The data we have found with testing the single unit may not scale up appropriately when connecting multiple units. In addition, smaller scales may prove to be less economical than larger, commercial-scale applications. The next steps in this project involve connecting and testing multiple units of the device, as well as testing it on larger applications such as a CNC machine to determine the increase in power seen. The power density produced by this prototype was far too small to be used in most applications. Further testing could look into changing the capacitor or battery chosen as another way to improve the power output.

Overall, this project has proved the concept that harvesting vibrational energy can be incorporated into household items. Within the next few years, advancements in technology may allow harvesting devices to have more versatility in terms of application. With more advancements in technology, devices such as the one for this project will be more economically feasible.

References

- [1] “Climate change causes: A blanket around the Earth,” *NASA*, 08-Aug-2018. [Online]. Available: <https://climate.nasa.gov/causes/>. [Accessed: 11-Oct-2018].
- [2] D. Glick, “The Big Thaw,” *Global Climate Change, Melting Glaciers*, 18-Jan-2017. [Online]. Available: <https://www.nationalgeographic.com/environment/global-warming/big-thaw/>. [Accessed: 11-Oct-2018].
- [3] F. Witsil, “Pros, cons of renewable energy sources,” *Detroit Free Press*, 11-Oct-2015. [Online]. Available: <https://www.freep.com/story/money/business/2015/10/10/renewable-energy-sources/73611806/>. [Accessed: 11-Oct-2018].
- [4] S. P. Beeby and T. O’Donnell, “Electromagnetic Energy Harvesting,” *SpringerLink*, 01-Jan-1970. [Online]. Available: https://link.springer.com/chapter/10.1007/978-0-387-76464-1_5. [Accessed: 11-Oct-2018].
- [5] “Reviving Vibration Energy Harvesting and Self-Powered Sensing by a Triboelectric Nanogenerator,” *Joule*, 04-Oct-2017. [Online]. Available: <https://www.sciencedirect.com/science/article/pii/S2542435117300776>. [Accessed: 11-Oct-2018].
- [6] G. B. Adams, “The Ideal Spring,” *public.asu.edu*, 2018.
- [7] R. Nave, Resonance. [Online]. Available: <http://hyperphysics.phy-astr.gsu.edu/hbase/Sound/reson.html>. [Accessed: 12-Oct-2018].
- [8] R. E. Blake, BASIC VIBRATION THEORY. [Online]. Available: https://www.accessengineeringlibrary.com/browse/harris-shock-and-vibration-handbook-sixth-edition/p200193b599702_1001. [Accessed: 12-Oct-2018].
- [9] Electrostatic kinetic energy harvesting (Phillippe Basset, Elena Blokhina, Dimitri Galayko) (ISTE, WILEY)
- [10] Ø. N. Dahl “How Does A Capacitor Work?,” *Build Electronic Circuits*, 19-sep-2013. [Online]. Available: <https://www.build-electronic-circuits.com/how-does-a-capacitor-work/>. [Accessed: 26-Oct-201].
- [11] “How do capacitors work?,” *Explain that Stuff*, 30-Mar-2018. [Online]. Available: <https://www.explainthatstuff.com/capacitors.html>. [Accessed: 22-Oct-2018].
- [12] R. T. Aljadiri, L. Y. Taha, and P. Ivey, “Electrostatic Energy Harvesting Systems: A Better Understanding of Their Sustainability ,” *Journal of Clean Energy Technologies*, vol. 5, no. 5, pp. 409–416, Sep. 2017.[Online]. Available: <http://www.jocet.org/vol5/407-RB006.pdf>
- [13]“Electric Current,” *The Physics Classroom*. [Online]. Available: <https://www.physicsclassroom.com/class/circuits/Lesson-2/Electric-Current>. [Accessed: 22-Nov-2018].

- [14] *Understanding Electricity - Learn about electricity, current, voltage and resistance*. [Online]. Available: http://www.leonics.com/support/article2_2j/articles2_2j_en.php. [Accessed: 22-Oct-2018].
- [15] “Harvard Natural Sciences Lecture Demonstrations,” *Bird on a High-Voltage Transmission Line*. [Online]. Available: <https://sciencedemonstrations.fas.harvard.edu/presentations/triboelectric-effects>. [Accessed: 01-Feb-2019].
- [16] B. W. Lee and D. E. Orr, “The Triboelectric Series - AlphaLab, Inc,” *AlphaLab, Inc*. [Online]. Available: <https://www.alphalabinc.com/triboelectric-series/>. [Accessed: 22-Feb-2019].
- [17] S. Niu and Z. L. Wang, “Theoretical systems of triboelectric nanogenerators,” *Nano Energy*, vol. 14, pp. 161–192, May 2015. [Online]. Available: http://www.nanoscience.gatech.edu/paper/2015/15_NE_11.pdf
- [18] J. Peng, S. D. Kang, and G. J. Snyder, “Optimization principles and the Figure of merit for triboelectric generators,” *Science Advances*, 01-Dec-2017. [Online]. Available: <http://advances.sciencemag.org/content/3/12/eaap8576>. [Accessed: 08-Oct-2018]
- [19] J. Toon, “Capturing wasted electricity with triboelectric generators,” *Phys.org - News and Articles on Science and Technology*, 10-Dec-2013. [Online]. Available: <https://phys.org/news/2013-12-capturing-electricity-triboelectric.html>. [Accessed: 22-Nov-2018].
- [20] C. R. Saha, *Optimization of an Electromagnetic Energy Harvesting Device - IEEE Journals & Magazine*. [Online]. Available: <https://ieeexplore.ieee.org/abstract/document/1704676>. [Accessed: 11-Oct-2018].
- [21] V. Challa, “A coupled piezoelectric–electromagnetic energy harvesting technique for achieving increased power output through damping matching,” [Online]. Available: <http://iopscience.iop.org/article/10.1088/0964-1726/18/9/095029/meta>, 06-Aug-2009.
- [22] “Piezoelectricity Harvesting.” [Online]. Available: <https://publish.illinois.edu/npre201piezo-fall2012/history-background/>. [Accessed: 08-Oct-2018].
- [23] A. Ledoux, “Theory of Piezoelectric Materials and Their Applications in Civil Engineering,” 24-Jun-2011. [Online]. Available: <https://dspace.mit.edu/bitstream/handle/1721.1/66839/757753448-MIT.pdf?sequence=2>. [Accessed: 08-Oct-2018].
- [24] E. Ghafari, S. Ghahari, Y. Feng, and N. Lu, “Piezoelectricity & Its Applications ,” 2016. [Online]. Available: [https://www.purdue.edu/discoverypark/energy/documents/2016 Guest Presentations/Luna Lu - Piezoelectric Materials and Devices - 2016 Energy Academy.pdf](https://www.purdue.edu/discoverypark/energy/documents/2016%20Guest%20Presentations/Luna%20Lu%20-%20Piezoelectric%20Materials%20and%20Devices%20-%202016%20Energy%20Academy.pdf). [Accessed: 08-Oct-2018].
- [25] Libretexts, “Dipole-Dipole Interactions,” *Chemistry LibreTexts*, 30-Jan-2017. [Online]. Available: [https://chem.libretexts.org/Textbook_Maps/Physical_and_Theoretical_Chemistry_Textbook_Maps/Supplemental_Modules_\(Physical_and_Theoretical_Chemistry\)/Physical_Properties_of_Matt](https://chem.libretexts.org/Textbook_Maps/Physical_and_Theoretical_Chemistry_Textbook_Maps/Supplemental_Modules_(Physical_and_Theoretical_Chemistry)/Physical_Properties_of_Matt)

er/Atomic_and_Molecular_Properties/Intermolecular_Forces/Specific_Interactions/Dipole-Dipole_Interactions. [Accessed: 08-Oct-2018].

[26] F. Cottone, “Introduction to Vibration Energy Harvesting,” Aug-2011.

[27] V. Kulkarni, R. B. Mrad, T. El-Diraby, and E. Prasad, “Energy Harvesting Using Piezoceramics,” *Volume 4: 12th International Conference on Advanced Vehicle and Tire Technologies*; 4th International Conference on Micro- and Nanosystems, 2010.

[28] Muensit, N. “Energy harvesting with piezoelectric and pyroelectric materials : Energy harvesting with piezoelectric and pyroelectric materials.” [Online]. Available: <https://ebookcentral-proquest-com.ezproxy.wpi.edu>

[29] S. Whitney, “Vibrations of Cantilever Beams: Deflection, Frequency, and Research Uses ,” *Motion of a Falling Ball*, 23-Apr-1999. [Online]. Available: <http://emweb.unl.edu/Mechanics-Pages/Scott-Whitney/325hweb/Beams.htm>. [Accessed: 22-Nov-2018].

[30] “Cantilever Beams - Moments and Deflections,” *Young's Modulus of Elasticity for Metals and Alloys*. [Online]. Available: https://www.engineeringtoolbox.com/cantilever-beams-d_1848.html. [Accessed: 18-Nov-2018].

[31] W. Shih, W.-H. Shih, and Z. Shen, “US20070089515A1 - Piezoelectric cantilever sensors,” *Google Patents*. [Online]. Available: <https://patents.google.com/patent/US20070089515>. [Accessed: 18-Oct-2018].

[32] L. Zyga, “Energy harvesting skin generates power from air conditioners,” *Phys.org - News and Articles on Science and Technology*, 20-Apr-2011. [Online]. Available: <https://phys.org/news/2011-04-energy-harvesting-skin-power-air.html>. [Accessed: 18-Oct-2018].

[33] P. Panthongsy, D. Isarakorn, P. Janphuang, and K. Hamamoto, “Fabrication and evaluation of energy harvesting floor using piezoelectric frequency up-converting mechanism,” *Sensors and Actuators*, vol. 279, no. 15, pp. 321–330, Aug. 2018. [Online]. Available: <https://www.sciencedirect.com/science/article/pii/S0924424717320095>

[34] Baldwin, J. D., Roswurm, S., Nolan, J., & Holliday, L. (2011). Energy harvesting on highway bridges (No. FHWA-OK-11-01). [Online]. Available: <https://shareok.org/bitstream/handle/11244/299430/FHWA-OK-11-01%202224%20Baldwin.pdf?sequence=1&isAllowed=y>

[35] T. W. Judson, “Resonance,” *The Ordinary Differential Equations Project*. [Online]. Available: <http://faculty.sfasu.edu/judson/w/ode/html/secondorder04.html>.

[36] E. Vanz and J. Karakiewicz, “Pedestrian as Generator: Implementing a Stand-Alone Piezo Power Generating Device in the Urban Context,” *Communications in Computer and Information Science Computer-Aided Architectural Design Futures. The Next City - New Technologies and the Future of the Built Environment*, pp. 154–171, 2015. [Online]. Available: https://link.springer.com/chapter/10.1007/978-3-662-47386-3_9

[37] Thomson, W. (2018). *Theory of vibration with applications*. CrC [Online]. Available: Press.file:///C:/Users/lrcarlson/AppData/Local/Packages/MicrosoftEdge_8wekyb3d8bbwe/TempState/Downloads/9780203718841_googlepreview.pdf

- [38] Notes, E. (n.d.). Diode Rectifier Circuits. Retrieved from https://www.electronics-notes.com/articles/analogue_circuits/diode-rectifiers/circuits-basics-primer.php#
- [39] Full Wave Rectifier and Bridge Rectifier Theory. (2019, January 29). Retrieved from https://www.electronics-tutorials.ws/diode/diode_6.html
- [40] Teo, W. (2016). *Electrospun membrane for triboelectric power generation*. [online] Electrospintech.com. Available at: <http://electrospintech.com/triboelectric.html#.XGMk3VxKiUk>.
- [41] “AC Motor,” *Total Internal Reflection*. [Online]. Available: <http://hyperphysics.phy-astr.gsu.edu/hbase/magnetic/motorac.html>. [Accessed: 22-Nov-2018].
- [42] “Controlling Machine Vibration And Shock,” *Production Machining*, 15-Jan-2003. [Online]. Available: <https://www.productionmachining.com/articles/controlling-machine-vibration-and-shock>. [Accessed: 22-Oct-2018].
- [43] “Why Reducing Machine Vibration Is Important for Maximum Efficiency,” *Sorbothane / Innovating Shock and Vibration Solutions*. [Online]. Available: <https://www.sorbothane.com/machine-vibration-reduction.aspx>. [Accessed: 10-Feb-2019].
- [44] “Reducing noise and vibration from machine tools,” *Noise & Vibration Worldwide*, vol. 47, no. 9-11, pp. 133–139, Oct. 2016. Retrieved from <https://journals.sagepub.com/doi/full/10.1177/0957456516683013>
- [45] “Solutions For Industrial Facilities Noise Control and Vibration Isolation,” *Kinetics Noise Control*. [Online]. Available: <https://kineticsnoise.com/industrial/pdf/industrial.pdf>.
- [46] Chang, M. L., Lin, C. C., Ueng, J. M., Hsieh, K. H., & Wang, J. F. (2010). Experimental study on adjustable tuned mass damper to reduce floor vibration due to machinery. *Structural Control and Health Monitoring*, 17(5), 532-548. [Online]. Available: <https://onlinelibrary.wiley.com/doi/pdf/10.1002/stc.330>
- [47] “Triboelectric Nanogenerator,” *Nano Electron. Sci. & Eig. Lab (NESEL)*. [Online]. Available: <http://nesel.skku.edu/generators.html>. [Accessed: 22-Feb-2019].
- [48] “ABB Robotics,” *ABB*. [Online]. Available: <https://new.abb.com/products/robotics/>. [Accessed: 22-Feb-2019].
- [49] “London Business Angels,” *Syndicate Room*. [Online]. Available: <https://www.syndicatoroom.com/angel-investors/networks/london-business-angels>. [Accessed: 23-Feb-2019].
- [50] “Pavegen - The Next Step,” *Pavegen - The Next Step*. [Online]. Available: <http://www.pavegen.com/>. [Accessed: 23-Feb-2019].
- [51] P. Mitcheson, E. Yeatman, G. Rao, A. Holmes, and T. Green, “Energy Harvesting From Human and Machine Motion for Wireless Electronic Devices,” *Proceedings of the IEEE*, vol. 96, no. 9, pp. 1457–1486, 2008.

- [52] “Difference Between Damped and Undamped Vibration,” *Pediaa.Com*, 28-Oct-2015. [Online]. Available: <http://pediaa.com/difference-between-damped-and-undamped-vibration/>. [Accessed: 01-Mar-2019].
- [53] Rex Plastics, “How Much Do Injection Molds Cost?,” *Rex Plastics*, 10-Jul-2017. [Online]. Available: <https://rexplastics.com/plastic-injection-molds/how-much-do-plastic-injection-molds-cost>. [Accessed: Feb-2019].
- [54] “11 Ways to Reduce Injection Molding Costs | Design Tip,” *Protolabs*. [Online]. Available: <https://www.protolabs.com/resources/design-tips/11-tips-to-reduce-injection-molding-costs/>. [Accessed: 01-Mar-2019].
- [55] C. Knight, J. Davidson, and S. Behrens, “Energy Options for Wireless Sensor Nodes,” *Current neurology and neuroscience reports.*, 08-Dec-2008. [Online]. Available: <https://www.ncbi.nlm.nih.gov/pubmed/27873975>. [Accessed: Feb-2019].
- [56] H. G. Craighead, “Nanoelectromechanical Systems,” *Science*, 24-Nov-2000. [Online]. Available: <http://science.sciencemag.org/content/290/5496/1532>. [Accessed: 01-Mar-2019].
- [57] “PCB Orders,” *ESP-WROOM-32 (ESP32 WiFi-BT-BLE MCU Module)*. [Online]. Available: https://www.elecrow.com/pcb-manufacturing.html?find=0&layer=4&size_x=127&size_y=127&quantity=1000&bcountnum=1000&designs=1&land=1.6&color=Green&charcolor=White&spray=HASL&bankong=0&copper=1&insidcopper=&sendtime=11. [Accessed: 01-Mar-2019].
- [58] *Thorlabs -Co-Fired Piezoelectric Actuators, 4.6 μm to 17.4 μm Travel*. [Online]. Available: https://www.thorlabs.com/newgrouppage9.cfm?objectgroup_id=61. [Accessed: 22-Feb-2019].
- [59] *Thorlabs - HEP3965 Broadband IR Tungsten Bulb, 1900 K, TO-8 Can*. [Online]. Available: https://www.thorlabs.com/newgrouppage9.cfm?objectgroup_id=61. [Accessed: Mar-2019].
- [60] M. S. Mohd Resali and H. Salleh, “Development of Multiple-Input Power Management Circuit for Piezoelectric Harvester,” *Mechanical Engineering*, vol. 2, pp. 215–230, 2017
- [61] F. Yildiz, “Potential Ambient Energy-Harvesting Sources and Techniques,” *Journal of Technology Studies*, vol. 35, no. 1, pp. 40–48, 2009. [Online]. Available: <https://eric.ed.gov/?id=EJ888131>
- [62] S. P. Beebly, M. J. Tudor, and N. M. White, “Energy harvesting vibration sources for microsystems applications,” *Measurement Science and Technology*, vol. 17, no. 12, pp. 175–195, Oct. 2006.
- [63] S. Rafique, *Piezoelectric Vibration Energy Harvesting: Modeling & Experiments*. Cham: Springer International Publishing, 2018.
- [64] W. by AZoNano, “Nanoelectromechanical Systems (NEMS) - Introduction, Application and Challenges of Nanoelectromechanical Systems,” *AZoNano.com*, 31-Jul-2017. [Online]. Available: <https://www.azonano.com/article.aspx?ArticleID=2465>. [Accessed: Mar-2019].

[65] S. Mishra, L. Unnikrishnan, S. K. Nayak, and S. Mohanty, “Advances in Piezoelectric Polymer Composites for Energy Harvesting Applications: A Systematic Review,” *Macromolecular Materials and Engineering*, vol. 304, no. 1, p. 1800463, 2018.

[66] *Three-Axis Accelerometer Evaluation Board*. Available: <https://www.analog.com/media/en/technical-documentation/evaluation-documentation/EVAL-ADXL326Z.pdf>.

Appendices

Appendix A: Blender Motor Speed Test Procedure

The purpose of this test procedure is to measure and record each of the blender motor speeds. The data collected can be used to determine the range of speeds the motor will operate at, in addition to identifying any correlation between the speed and frequency the blender vibrates at.

A digital tachometer is used to measure the rotational speed of the blender. There is an assumption that the rotational speed correlates relatively well with the speed of the motor based on the simple geography of the motor and shaft. The digital tachometer that will be used is the neiko digital tachometer 20713A. This instrument measures in the range of 2.5-99,999 RPM. The resolution is 0.1RPM for the range of 2.5-999.9RPM and resolution of 1RPM for over 1000 RPM. The sampling time is 0.8 sec (over 60 RPM). It also measures RPM with an accuracy of 0.05% when the device is positioned within 2-20 inches of the object rotating.

Measuring Procedure:

1. Cut a small piece of the reflective marker and apply it to the object being measured. Measure the reflective marker to be approximately a 12mm square. It is important that the non-reflective area remains larger than the reflective area to obtain accurate results. It is also very important that the shaft is not reflective itself, otherwise it will need to be covered with black tape or paint. The reflective marker must stand out from the rotating shaft in order for the instrument to work.
2. Apply the reflective marker to the top of the blender base as shown in the Figure below. Using a caliper measure from the center point of the reflective marker to the center point of the rotating blender base, as shown in Figure 33 below and record the distance.



Figure 33: Visual Diagram of Marker and Radius

3. Setup a timer for 6 seconds and align the laser with the reflective marker. To do this, hold the device approximately 6 inches above the marker.
4. Have a partner start the timer as well as the speed at which the test will be performed. Wait until the end of the first second of the motor being on to hold down the Test button. Continue to hold the test button for the remaining 5 seconds. At the end of these 5 seconds release the test button.
5. Using the Mem button, retrieve the data stored from the latest trial. Click the button once for the maximum value. Click the button twice to retrieve data about the minimum value and click it a third time to record the data from the final measurement.
6. Repeat for each speed 5 total trials: Chop, Mix, Grate, Blend, and Liquefy.
7. The Pulse speed trials for testing are measured differently. Begin recording the tachometer then press the pulse button once. Record through the entire pulse.
8. Repeat step 7 for 5 total trials
9. Average each of the trials for maximum value, minimum value, and final value recorded.

The complete data that we got from this experiment is shown below:

Table 9: Full Tachometer Data

Chop (5sec)	RPM			Mix (5sec)	RPM			Grate (5sec)	RPM		
Blender Speed	Max	Min	Final	Blender Speed	Max	Min	Final	Blender Speed	Max	Min	Final
<i>Trial 1</i>	18699	18154	18266	<i>Trial 1</i>	21939	18889	18946	<i>Trial 1</i>	21091	19376	19449
<i>Trial 2</i>	19356	18091	18329	<i>Trial 2</i>	19002	12878	19002	<i>Trial 2</i>	19542	19192	19526
<i>Trial 3</i>	18883	18244	18335	<i>Trial 3</i>	18963	18939	18939	<i>Trial 3</i>	19473	19382	19473
<i>Trial 4</i>	18372	18248	18356	<i>Trial 4</i>	19157	19059	19059	<i>Trial 4</i>	20583	19410	19500
<i>Trial 5</i>	18425	18214	18264	<i>Trial 5</i>	19152	19068	19092	<i>Trial 5</i>	20226	19351	19351
Average	18747	18190	18310	Average	19643	17767	19008	Average	20183	19342	19460

Blend (5sec)	RPM			Liquify (5sec)	RPM			Pulse (*)	RPM		
Blender Speed	Max	Min	Final	Blender Speed	Max	Min	Final	Blender Speed	Max	Min	Final
<i>Trial 1</i>	21411	19869	19976	<i>Trial 1</i>	20813	20003	20146	<i>Trial 1</i>	9347.0	88.400	3131.0
<i>Trial 2</i>	21603	19942	20011	<i>Trial 2</i>	20185	20029	20161	<i>Trial 2</i>	9736.0	6742.0	6742.0
<i>Trial 3</i>	22193	19902	20010	<i>Trial 3</i>	20099	19992	20099	<i>Trial 3</i>	6468.0	396.90	3700.0
<i>Trial 4</i>	20496	19890	20029	<i>Trial 4</i>	20183	20091	20183	<i>Trial 4</i>	10734	7893.0	7893.0
<i>Trial 5</i>	20168	19829	19995	<i>Trial 5</i>	20244	20083	20203	<i>Trial 5</i>	10850	8280.0	8280.0
Average	21174	19886	20004	Average	20305	20040	20158	Average	9427.0	4680.1	5949.2

Appendix B: Accelerometer Test Procedure

The purpose of this test procedure is to measure and record the accelerations from the vibrations of a blender. The data that is collected will be used to calculate the maximum deflection from the accelerations, which will provide information on purchasing the appropriate range of piezoelectric devices for the final design.

In this experiment a 6-speed blender is used in conjunction with a MEMs 3 Axis accelerometer to record acceleration measurements for each of the axis (X, Y, and Z) via a LabVIEW program. The first part of the test procedure outlines the preliminary setup for the experiments. The second and third part outlines testing the blender with a cornstarch solution and water, respectfully. The last part focuses on changing the placement of the accelerometer onto the prototype design.

Preliminary Setup

Blender

In the following experiments the 6-Speed Blender from MAINSTAYS is used. The blender can be seen below in Figure 34 This is a 350 Watt motor that should be used in a 120-volt 60Hz AC outlet. The 6 different speeds are as follows: Chop, Mix, Grate, Blend, Liquefy, and Pulse.



Figure 34: 6-Speed Blender from MAINSTAYS

Accelerometer

This procedure references a 3 axis EVAL-ADXL326Z-ND sensor evaluation board. This device is low noise, drift, and power, and will be used along with a LabVIEW program to measure the vibration of the blender in all 3 axis (X, Y, and Z). The pins that will be used to obtain this data are shown in Figure 35:

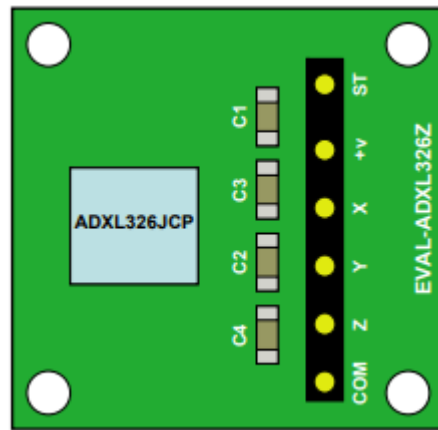


Figure 35: ADXL326Z Sensor Board

The ADXL326Z accelerometer supports accelerations within the minimum range of $\pm 16g$. The sensitivity for this range is typically 57 mV/g. In addition during testing, the power supply should never exceed 3.6 V or there is a potential to damage the device. The analog output signals are voltages that are proportional to acceleration. Orientation of the sensor is shown in Figure 36 along with a depiction of the expected output response for each of the possible orientations. These depictions will assist one in calibrating the accelerometer based on the orientation and axis being measured.

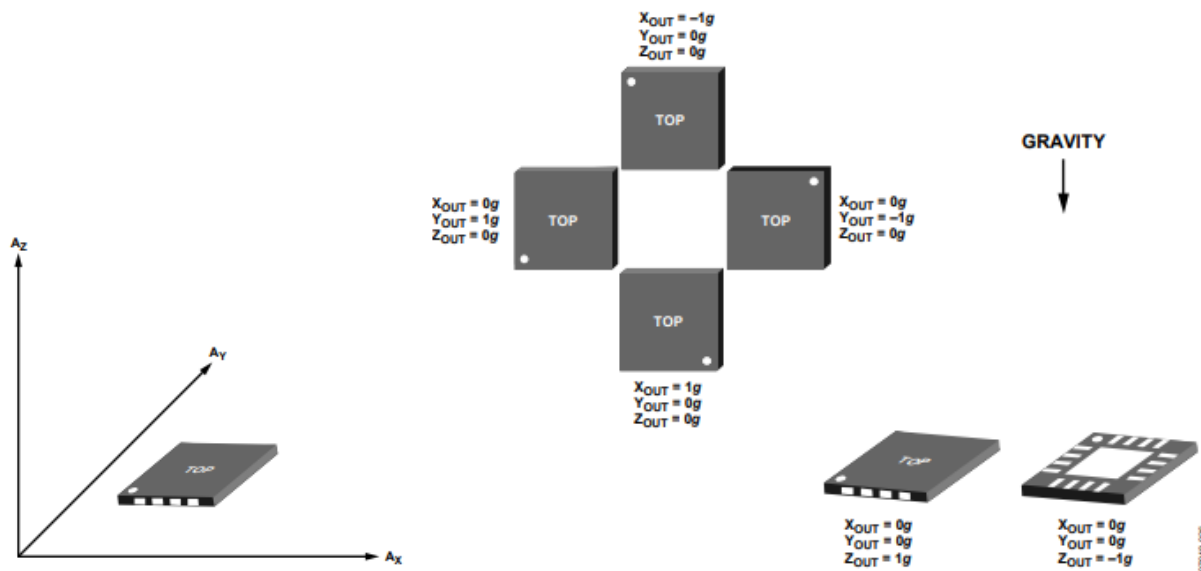


Figure 36: Axis of Orientation and Sensitivity to Gravity

National Instruments DAQ Box

Data acquisition (DAQ) is used to measure the electrical voltage from the output of the accelerometer. The model number of the DAQ box is USB 6229. Data from the DAQ box is measured and used in the following LabVIEW.

LabVIEW Program

LabVIEW is a laboratory virtual instrument engineering workbench that can be used to interpret the voltage data the accelerometer outputs in addition to supplemental calculations. For example, LabVIEW can calculate the fast Fourier transform (FFT) to record frequency.

The purpose of the LabVIEW in this experiment is to record acceleration values. The LabVIEW program inputs the voltage from the accelerometer and manipulates the data based on the voltage to acceleration ratio. The program also allows the user to change the voltage offset to calibrate the device.

Assembling the System Circuit

The circuit connecting the system will use two BNC cables, two BNC to a split banana connector, two banana cables, and an external battery supply setup. This setup focuses on reading a single axis of acceleration using differential signaling. Differential signaling is advantageous because there is no current return and because it has better resistance to electromagnetic interference and crosstalk.

Attach the two BNC cables to the DAQ Box Analog Inputs so that the LabVIEW program recognizes what inputs are active as can be seen in Figure 37. Then attach the two BNC cables that have a split banana connector.

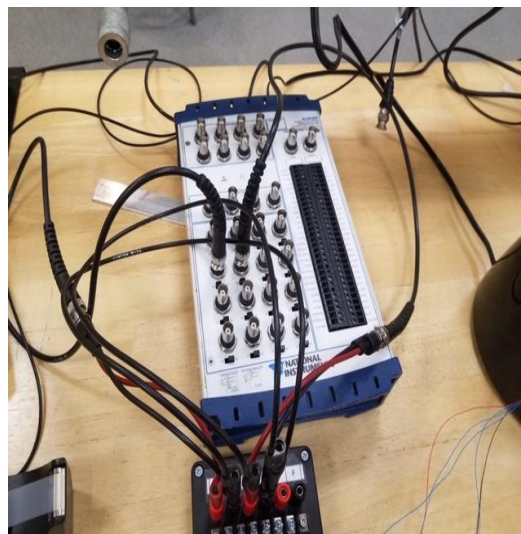


Figure 37: BNC Connection to DAQ Box

Using a connection box, as shown in Figure 38, create connections between the accelerometer and DAQ box. Create a connection for common ground between all cables.

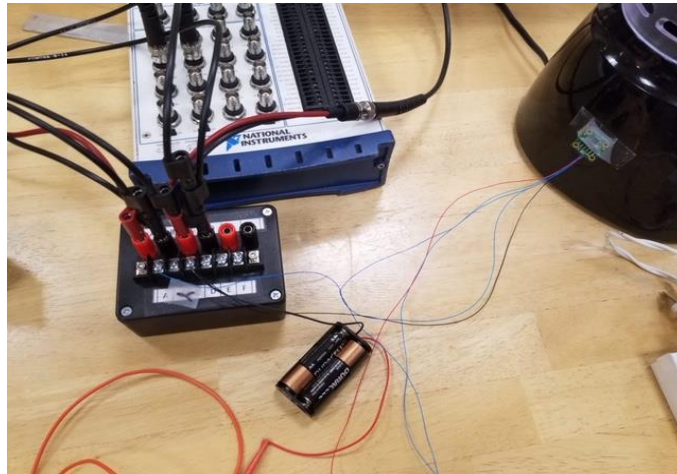


Figure 38: Connections between Accelerometer and DAQ Box

Use an external battery source to create the connections necessary to supply power to the accelerometer. By supplying an external source rather than having the DAQ box do so, the output signal from the accelerometer will be have less noise. The setup for the external power source is depicted in Figure 39:

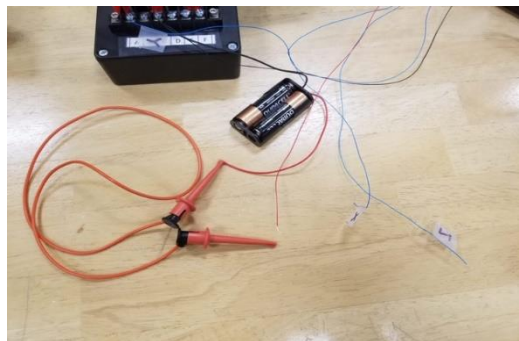


Figure 39: External Battery Source for Accelerometer

Experimental Testing with Cornstarch

The purpose of this section is to determine the significance between each of the speed settings on the blender. The acceleration values that are recorded will be used to calculate the RMS value for each trial run and recorded for comparison between all settings and axis.

Position 1:

1. Place the accelerometer on the side of the bottom base of the blender.
2. Add 32 ounces of water and 20 tablespoons of cornstarch into the blender and secure the lid.

3. Ensure the blender top is securely mounted to its base and plug the blender into the wall outlet.
4. In the save file box of the LabVIEW program save an empty excel sheet as “Test Data” (make sure it is saved as an Excel 1993-2007 Workbook).
5. Attach the X-Axis wire.
6. Start the LabVIEW Program.
7. Adjust the calibration value on the front panel of the program so the acceleration graph reads zero. (There should only be a small amount of noise, about ± 0.05 g.)
8. Turn blender on “blend” setting and let run for 5 seconds.
9. Begin recording on the LabVIEW and let run for 10 seconds.
10. Stop recording and turn LabVIEW program off and then turn the blender off.
11. Open the data file and save the data file with an appropriate name (XAxis_Cornstarch_Trial1) into a different location. Be sure to save the file as a workbook excel file.
12. Repeat steps 8-11 twice more.
13. Repeat steps 5-12 for the Y-Axis and Z-Axis.
14. Repeat steps 5-13 for each blender setting.

With the data collected from above (Position 1 with cornstarch) calculate the RMS. Record these values in a table and average each of the trials.

Position 2:

1. Place the accelerometer on the bottom of the blender.
2. Repeat steps 1-14 done previously for position 1.
3. Calculate and record the RMS value for the acceleration for each trial.

Experimental Testing with Water

As a result of testing and comparing the results from the RMS table in the previous section, the Liquefy setting on the blender provided the highest RMS value. The liquefy setting will be tested in this section.

Position 1:

1. Place the accelerometer on the side of the bottom base of the blender.
2. Add 32 ounces of water into the blender and secure the lid.
3. Ensure the blender top is securely mounted to its base and plug the blender into the wall outlet.
4. In the save file box of the LabVIEW program save an empty excel sheet as “Test Data” (make sure it is saved as an Excel 1993-2007 Workbook).
5. Attach the X-Axis wire.
6. Start the LabVIEW Program.

7. Adjust the calibration value on the front panel of the program so the acceleration graph reads zero. (There should only be a small amount of noise, about ± 0.05 g.)
8. Turn blender on “blend” setting and let run for 5 seconds.
9. Begin recording on the LabVIEW and let run for 10 seconds.
10. Stop recording and turn LabVIEW program off and then turn the blender off.
11. Open the data file and save the data file with an appropriate name (XAxis_Cornstarch_Trial1) into a different location. Be sure to save the file as a workbook excel file.
12. Repeat steps 8-11 twice more.
13. Repeat steps 5-12 for the Y-Axis and Z-Axis.

Position 2:

1. Place the accelerometer on the bottom of the blender.
2. Repeat steps 1-13 done previously in this section for position 1.

Experimental Testing with Accelerometer on Prototype

This part of the procedure follows the steps from the previous section, but with changes in the placement of the accelerometer onto the prototype. Place accelerometer on the edge of the supportive plate that lies on top of the ball bearings. Use a hot glue gun to make a rigid connection between the device and design. Make note of the orientation of the axis. In this section, the vertical axis will be recorded.

Testing with Water:

1. Add 32 ounces of water into the blender and secure the lid.
2. Ensure the blender top is securely mounted to its base and plug the blender into the wall outlet.
3. In the save file box of the LabVIEW program save an empty excel sheet as “Test Data” (make sure it is saved as an Excel 1993-2007 Workbook).
4. Attach the Z-Axis wire.
5. Start the LabVIEW Program.
6. Adjust the calibration value on the front panel of the program so the acceleration graph reads zero. (There should only be a small amount of noise, about ± 0.05 g.)
7. Turn blender on “blend” setting and let run for 5 seconds.
8. Begin recording on the LabVIEW and let run for 10 seconds.
9. Stop recording and turn LabVIEW program off and then turn the blender off.
10. Open the data file and save the data file with an appropriate name (XAxis_Cornstarch_Trial1) into a different location. Be sure to save the file as a workbook excel file.
11. Repeat steps 8-11 twice more.

Testing with Cornstarch:

1. Add 32 ounces of water and 20 tablespoons of cornstarch into the blender and secure the lid.
2. Repeat steps 1-11 done previously in this section for testing with water.
3. Compare these results to the results when the accelerometer was placed on the blender to understand the efficiency of the system due to the design's frictional energy loss.

Appendix C: Piezoelectric Test Procedure for Voltage Testing

The purpose of this test procedure is to measure and record the voltage output from the assembled prototype, while recording the accelerations produced by the vibrations. In this experiment a 6-speed blender is used to test the designed prototype. The first section of the test procedure outlines the preliminary setup of the accelerometer on the blender that will be used for the following experiments. The following section outlines how the data should be measured and recorded from the experimental setup.

Preliminary Setup

Accelerometer:

1. Position the 3 axis EVAL-ADXL326Z-ND sensor evaluation board on the side of the bottom base of the blender. This is the same as position one used in the experimental blender test procedure.

LabVIEW Program:

1. Reference the previous LabVIEW program that was used to record the acceleration values in the blender test procedure.
2. Add another feature to the LabVIEW program to record the voltage

Experimental Testing

This part of the test procedure tests the final prototype with water as well as a cornstarch solution in the blender.

Testing with Water:

1. Add 32 ounces of water into the blender and secure the lid.
2. Ensure the blender top is securely mounted to its base and plug the blender into the wall outlet.
3. Place the entire blender on top of the prototype plate.
4. Attach the wires from the breadboard to DAQ assistant using BNC connectors and alligator clips.
5. In the save file box of the LabVIEW program save an empty excel sheet as “Test Data” (make sure it is saved as an Excel 1993-2007 Workbook).
6. Attach the Z-Axis wire.
7. Start the LabVIEW Program.
8. Adjust the calibration value on the front panel of the program so the acceleration graph reads zero. (There should only be a small amount of noise, about ± 0.05 g.)
9. Turn blender on the “Liquefy” setting and let run for 5 seconds.
10. Click the “Start Recording” button on the LabVIEW and let run for 10 seconds.
11. Stop recording and turn LabVIEW program off and then turn the blender off.

12. Open the data file and save the data file with an appropriate name (ZAxis_Water_Trial1) into a different location. Be sure to save the file as a workbook excel file.
13. Repeat steps 8-13 twice more.

Testing with Cornstarch:

1. Add 32 ounces of water and 20 tablespoons of cornstarch into the blender and secure the lid.
2. Repeat steps 2-13 done previously for testing with water.
3. Compare the final results

Appendix D: Specifications Sheets

THORLABS

435 Route 206 • P.O. Box 366
Newton, NJ 07860-0366

PH. 973-579-7227
FAX 973-300-3600

AE0505D08F SPECIFICATION SHEET

CAUTION:

**POLARITY MATTERS! RED LEAD ATTACHES TO +V,
WHITE LEAD ATTACHES TO GROUND (GND)!**

The AE0505D08F piezoelectric stack sold by Thorlabs is manufactured by NEC Corporation of Japan. These stacks consist of many piezoelectric ceramic layers that are assembled in series mechanically and in parallel electrically. To operate, connect the red lead of the device to the positive (+) terminal of the voltage source. Do not reverse bias.

I. SPECIFICATIONS

Displacement at Maximum Drive Voltage: 9.1 μ m +/- 1.5
Maximum Drive Voltage (short term): 150 volts (apply positive voltage to red lead, reverse bias will destroy this device)

Displacement at Recommended Drive Voltage: 6.1 μ m +/- 1.5
Recommended Drive Voltage: 100 volts

Operating Temperature Range: -25 to +85°C
Capacitance: 0.75 μ F +/- 20%
Clamping Force: 850 N
Tensile Strength: 85 N
Resonant Frequency: 138 KHz (no mechanical load)
Young's Modulus: 4.4 x 10¹⁰ N/m²
Recommended Preload: <425 N

AC or Pulsed operation causes the device to generate heat (see Figure 1).

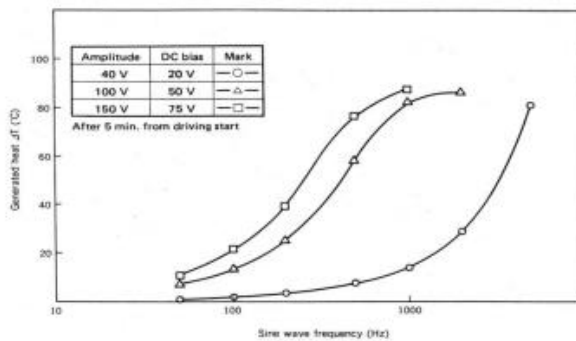


Figure 1- Sine wave Frequency vs. Generated Heat

15641-S01 Rev E, 3/28/11
Page 1 of 2

II. MEAN TIME FAILURE

Under the most severe operating conditions (150 VDC, 40°C, 90 % Relative Humidity) the mean time to failure is 500 hours. When the piezoelectric is operated at the recommended operating conditions (100 VDC, 25°C, 60 % RH) the mean time to failure is increased to 24,500 hours.

The following formula predicts the mean time to failure in hours for specific operating parameters that are below the maximum allowed.

$$\text{Mean Time to Failure} = 500 \times (150/V)^{3.2} \times (90/RH)^{4.9} \times 1.5^{(40-T)/10}$$

V: drive voltage HR: relative humidity (for 60% HR=60)
T: Ambient Temperature

III. CAUTIONS

Connect red wires to (+) drive voltage, do not reverse bias.

Do not exceed 150 volts, it will decrease the life expectancy of the device and in extreme cases mechanical failure will result.

Use room temperature epoxy adhesive for mechanical assembly of device.

Do not store devices about 100°C.

Do not immerse in liquid.

Do not use the device around combustible gases or liquids.

Store devices in a dry place (less than 40 % RH).

Do not clean with organic solvents.

IV. ROHS Compliance Statement:

The AE0505D08F Piezoelectric stack is considered "exempt" from ROHS compliance as of 7/1/06. While all connections to the stack are made with lead-free materials, the stack itself contains lead.

